

**EVALUATIVE TESTING OF A NOVEL WELDLESS  
OPEN STEEL GRID DECK SYSTEM**

by

**Matthew J. Pierce**

BS in Civil and Environmental Engineering, University of Pittsburgh, 2001

BS in Mathematics, Allegheny College, 1999

Submitted to the Graduate Faculty of  
School of Engineering in partial fulfillment  
of the requirements for the degree of  
Master of Science

University of Pittsburgh

2005

UNIVERSITY OF PITTSBURGH  
SCHOOL OF ENGINEERING

This thesis was presented

by

Matthew J. Pierce

It was defended on

December 5, 2005

and approved by

Dr. Jeenshang Lin, Associate Professor  
Department of Civil and Environmental Engineering

Dr. John F. Oyler, Adjunct Associate Professor  
Department of Civil and Environmental Engineering

Thesis Director: Dr. Christopher J. Earls, Associate Professor and Chairman  
Department of Civil and Environmental Engineering

Copyright © by Matthew J. Pierce

2005

## **EVALUATIVE TESTING OF A NOVEL WELDLESS OPEN STEEL GRID DECK SYSTEM**

Matthew J. Pierce, M.S.

University of Pittsburgh, 2005

The current thesis is a complete viability investigation of a novel open steel grid deck system that is weldless. The performance of this innovative deck design is evaluated within the context of fatigue and ultimate strength. Such evaluation is based on results obtained from a testing program performed in the Structures Laboratory at the University of Pittsburgh. A description of the deck system and testing methods, as well as a discussion of results is presented.

## TABLE OF CONTENTS

PREFACE.....	x
CHAPTER	
1.0 INTRODUCTION.....	1
1.1 OPEN GRID DECKS.....	1
1.2 RESEARCH OBJECTIVE.....	2
2.0 BACKGROUND.....	3
3.0 DESCRIPTION OF SPECIMEN.....	7
3.1 GEOMETRY.....	7
3.2 MANUFACTURING TECHNIQUE.....	9
4.0 LABORATORY PROCEDURES.....	11
4.1 DESCRIPTION OF LOAD FRAME AND ACTUATORS.....	11
4.2 INSTRUMENTATION.....	12
4.3 DATA ACQUISITION.....	13
5.0 LOADING PROTOCOL AND TESTING PROGRAM.....	15
5.1 AASHTO LRFD SPECIFICATIONS.....	15
5.2 LOADING.....	16
5.2.1 Fatigue.....	16
5.2.2 Ultimate Strength.....	17

6.0 RESULTS AND DISCUSSION.....	18
6.1 FATIGUE TESTING.....	18
6.1.1 Stiffness Characteristics .....	18
6.1.2 Deflection Profiles.....	21
6.2 ULTIMATE STRENGTH TESTING .....	23
7.0 CONCLUSION.....	25
7.1 FATIGUE TESTING.....	25
7.2 ULTIMATE STRENGTH.....	26
7.3 RECOMMENDATIONS FOR FUTURE RESEARCH.....	26
APPENDIX A STRAIN GAUGE LOCATIONS AND OVERALL GEOMETRY .....	27
APPENDIX B LABORATORY PHOTOGRAPHS .....	30
APPENDIX C DATA BREAKDOWN AND ADDITIONAL RESULTS.....	34
BIBLIOGRAPHY .....	58

## LIST OF TABLES

Table 6.1 – Percent Change in Weldless Deck Stiffness.....	19
Table C1 – Deflection Data.....	38
Table C2 – Pre-Fatigue Main Bar Strains .....	39
Table C3 – Post-Fatigue Main Bar Strains.....	40
Table C4 – Main Bar Neutral Axis Data: TM6-BM25 .....	47
Table C5 – Main Bar Neutral Axis Data: TM7-BM24 .....	47
Table C6 – Main Bar Neutral Axis Data: TM9-BM22 .....	47
Table C7 – Main Bar Neutral Axis Data: TM10-BM21.....	50
Table C8 – Main Bar Neutral Axis Data: TM13-BM18.....	50
Table C9 – Main Bar Neutral Axis Data: TM15-BM16.....	50
Table C10 – Pre- and Post-Fatigue Cross Bar Strains.....	53
Table C11 – Cross Bar Neutral Axis Data: TC5-BC26.....	56
Table C12 – Cross Bar Neutral Axis Data: TC8-BC23.....	56

## LIST OF FIGURES

Figure 3.1 – Deck Plan View.....	7
Figure 3.2 – Deck Elevation .....	8
Figure 3.3 – Alternating Main Bar Cutouts.....	9
Figure 3.4 – Assembly Process.....	10
Figure 4.1 – Load Frame and Weldless Deck.....	11
Figure 4.2 – DCDT Elevation .....	13
Figure 5.1 – S-N Curve.....	16
Figure 6.1 – Deck Stiffness.....	19
Figure 6.2 – Neutral Axis Locations.....	20
Figure 6.3 – Pre- and Post-fatigue Deflection Profiles .....	22
Figure 6.4 – Weldless Grid Deck at Failure.....	24
Figure A1 – Deck Plan View and Strain Gauge Location.....	28
Figure A2 – Deck Elevation.....	29
Figure B1 – MTS 458 Controller and Data Acquisition System .....	31
Figure B2 – DCDT Stand and Circuit Board .....	31
Figure B3 – 25 Kip Actuator Used in Fatigue Testing.....	32
Figure B4 – Foot of Actuator Used in Applying Load.....	32
Figure B5 – 250 Kip Actuator and Failed Weldless Grid Deck.....	33

Figure B6 – Transverse Deflection Profile.....	33
Figure C1 – Deck Stiffness Plots: Locations 1 and 3.....	35
Figure C2 – Deck Stiffness Plots: Locations 4 and 5.....	36
Figure C3 – Stiffness Per Number of Cycles.....	37
Figure C4 – Strain Profiles: Main Bar, TM6-BM25.....	41
Figure C5 – Strain Profiles: Main Bar, TM7-BM24.....	42
Figure C6 – Strain Profiles: Main Bar, TM9-BM22.....	43
Figure C7 – Strain Profiles: Main Bar, TM10-BM21.....	44
Figure C8 – Strain Profiles: Main Bar, TM13-BM18.....	45
Figure C9 – Strain Profiles: Main Bar, TM15-BM16.....	46
Figure C10 – Main Bar Neutral Axis Location: TM6-BM25.....	48
Figure C11 – Main Bar Neutral Axis Location: TM7-BM24.....	48
Figure C12 – Main Bar Neutral Axis Location: TM9-BM22.....	49
Figure C13 – Main Bar Neutral Axis Location: TM10-BM21.....	51
Figure C14 – Main Bar Neutral Axis Location: TM13-BM18.....	51
Figure C15 – Main Bar Neutral Axis Location: TM15-BM16.....	52
Figure C16 – Strain Profiles: Cross Bar, TC5-BC26.....	54
Figure C17 – Strain Profiles: Cross Bar, TC8-BC23.....	55
Figure C18 – Cross Bar Neutral Axis Location: TC5-BC26.....	57
Figure C19 – Cross Bar Neutral Axis Location: TC8-BC23.....	57

## PREFACE

I would like to offer a few lines of acknowledgement to all those that have not only made this thesis (and MS degree) become a reality, but also influenced my life in spectacular ways. To my engineering mentor, Dr. Christopher Earls, whose influence to achieve a higher level of knowledge has been a driving force behind my academic endeavors. To the faculties and staffs of Allegheny College and the University of Pittsburgh, and my colleagues of DMJM+Harris who have and continue to reinforce the foundation of my engineering career. And to my parents, Keith and Barb, in whom I have always trusted for support and demand in reaching my fullest potential in life – Thank You.

Foremost and by far most important is my family – my children Taylor and Carson and my wife Lisa – whose patience and commitment to me, our family, and this cause has been without bounds. I *could not* have done this without you – I love you all from here to the moon and back!

## **1.0 INTRODUCTION**

### **1.1 OPEN GRID DECKS**

Steel grid decks have provided reliable riding surfaces and flooring systems for more than half a century. Since their introduction in the 1920's and 1930's (Gilmore, 1987), steel grid decks have been employed by the design industry in spanning bridge floorbeams and stringers; examples including the Oakland Bay Bridge, the Brooklyn Bridge, and the Verrazano Narrows Bridge utilize concrete filled steel grid decks. More locally, the Homestead High Level Bridge, the Rankin Bridge, and the Smithfield Street Bridge also use filled grid decks. Modern improvements in manufacturing, as well as developments in design, have revolutionized the grid deck industry in creating lighter and more efficient grid decks through better materials and tighter tolerances. Design engineers today are also afforded a variety of options from various grid geometries to steel decks that are weldless.

Traditional grid decks are composed of hot-rolled steel members (bar stock and rolled shapes) placed orthogonal to one another through punch-outs and welded at their intersections. Typically, such welded decks are used in concrete filled as well as open grid deck applications. Research has shown (Klippstein, 1993 Mangelsdorf, 1991) that welding intersecting members can result in deleterious effect on the fatigue life

characteristics within current steel grid deck designs. One interesting and recent development is that of open steel grid decks that are weldless.

The current thesis is a presentation of results from a full-scale test of a novel weldless open steel grid deck prototype manufactured by Stargrate Systems Incorporated. Research to date has focused primarily on concrete filled and welded open steel grid decks; with little interest in weldless products. Hence, the current research program serves to demonstrate the viability of this weldless deck design for application in design and construction.

## **1.2 RESEARCH OBJECTIVE**

The current thesis describes research, and discusses results from, a program aimed at evaluating the structural performance of a weldless open steel grid deck manufactured by Stargrate Systems Incorporated. The objective of this work is to characterize the fatigue life and ultimate strength response of the weldless grid deck for use in bridge applications. The program of study is experimental in nature and involves a full-scale testing configuration in which a prototype deck is evaluated.

## 2.0 BACKGROUND

To date, no available research has been conducted to focus on open steel grid decks that are weldless. Typically, the available research has sought to characterize the fatigue life and ultimate strength behavior of welded open steel grid decks and partially- and fully-filled grid decks. The term welded in this capacity refers to the puddle welds used to rigidly link grid deck main bars to secondary and/or tertiary bars, which are typically oriented parallel, orthogonal, and/or skewed to the main bars. Since these puddle welds represent fatigue-prone details within the grid deck, much of the available research has studied the impacts of these welded connections on the overall fatigue resistance of the grid decks. Various research has examined grid decks (in filled and unfilled configurations) with reduced weld sizes and with the welds completely eliminated; these tests, however, were performed to draw comparisons with their welded counterparts within the context of fatigue and ultimate strength. As previously noted, the current investigation focuses solely on the behavior of a weldless open steel grid deck.

Huang et al. (2001), of the University of Delaware, conducted extensive experimental, numerical, and analytical analyses aimed at providing better insight into the behavior of open steel grid decks. A number of open steel grids were examined including a standard 5" 4-way and a 5" 4-way with reduced welds. The reduced puddle

welds were estimated at a third of the standard weld size. As Huang maintains, the reduced welds can minimize manufacturing costs and help to minimize and/or inhibit crack initiation during fatigue (2001).

Huang's experimental research consisted of static, ultimate strength, and cyclic loading. After three cycles of static loading, the decks were taken to failure wherein the deck with reduced welds began to experience 'popping' of the welds at a load of 89 kN (20 kips). Despite this phenomenon, the failure mode was similar for all decks: with yielding commencing at the central main bar and propagating outward away from the point of load application.

The experimental results from Huang, for the deck with reduced welds, showed a significant relative decrease in the stiffness of the deck. Huang surmised that the stiffness of the welds influences the transverse distribution of load; based on main bar strains, the transverse stiffness decreased by 7% with the reduced welds (2001).

Skroback (1999), also of the University of Delaware, characterized the static and fatigue behavior of both welded and nonwelded open grid decks. Again here, the intent of examining the nonwelded deck was to determine the influence of the welds on the static behavior of the open grid. Tests demonstrated the welds improved the structural behavior of the decks by enhancing the transverse load distribution throughout the deck. Skroback also concluded that in the idealized conditions of the laboratory the fatigue resistance of the welded open steel grid decks met the requirements of AASHTO fatigue category A (1999).

The University of Pittsburgh engaged in an extensive research program in the late 1980's to the mid 1990's focused on evaluating the static, ultimate strength, and fatigue

characteristics of both open and filled grid decks (Mangelsdorf, 1991 et al.). Of particular importance to the current research is the conclusion drawn that the fatigue-prone details of filled grids can be classified as AASHTO fatigue category C; such details include the web punch-outs and the puddle welds (Klippstein, 1993). Additional conclusions from the three phases of research include:

- Experimental tests were conducted in pursuit of the notion that nonwelded decks may experience some irregular slip between bars during loading; hammer tests aimed at rattling the decks demonstrated no shifts of deflection (Mangelsdorf, 1991).
- The twisting stiffness of the nonwelded deck was shown to be at least as high as the welded counterpart; it was surmised that welding of the components has a negligible effect in this regard (Mangelsdorf, 1991).
- Mangelsdorf suggested that welding at the intersections (of deck components) has no particular advantage for static behavior, and in general welding at every intersection may be eliminated with no significant change in structural properties (1991).

Clearly, the aforementioned contradictory and non-complimentary results highlight the fact that additional research is required to improve our understanding of weldless open grid deck response. The current research endeavors to contribute to this end with the presentation of experimental testing results and analysis of the observed behavior. In addition, advancements in manufacturing techniques, and the need to reduce costs, will not only continue to drive the development of novel products such as the current

weldless open steel grid deck, but require continued research to validate such products for practical use in the design and construction industries.

### 3.0 DESCRIPTION OF SPECIMEN

#### 3.1 GEOMETRY

The full-scale deck specimen consisted of 20 main bars (longitudinal), spaced 3½" on center; and 28 cross bars (transverse), spaced 4.0" on center, perpendicular to the main bars. The main bars were 5" x ¼" x 9'-6" and the cross bars were 2½" x ¼" x 6', both fabricated from ASTM A36 steel flat stock and providing an overall assembled deck geometry of 9'-6" x 6'-0". A complete illustration can be found in Appendix A.

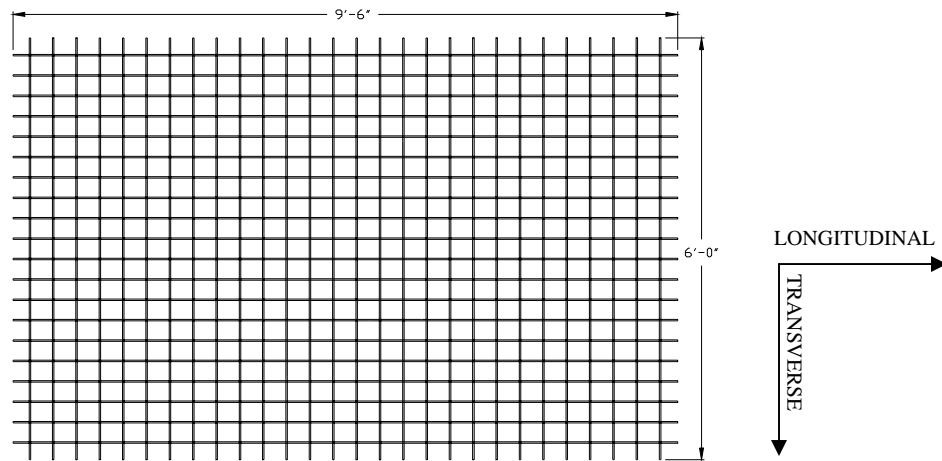


**Figure 3.1 - Deck Plan View**

Successive main bars contained alternating cutouts [Figure 3.2], providing the interlocking mechanism of the weldless deck. The notched cross bars were fabricated

to provide an interference fit in their connections with the main bars. The patterns for the cutouts were alternated in adjacent main bars to create a mechanically locked condition for the cross bars [See Figure 3.3].

The weldless grid deck was fabricated with  $\frac{3}{4}$ " round stock placed in three (3) locations at the quarter points of the longitudinal dimension [Figure 3.2]. The pieces of round stock served as locking pins to secure adjacent main bars in position. Since the locking bars were relatively stiff, in a flexural sense, it was thought that neutralizing all but the mid-span locking bar would make the test results easier to interpret. As a result, only the mid-span locking bar remained in place during testing.

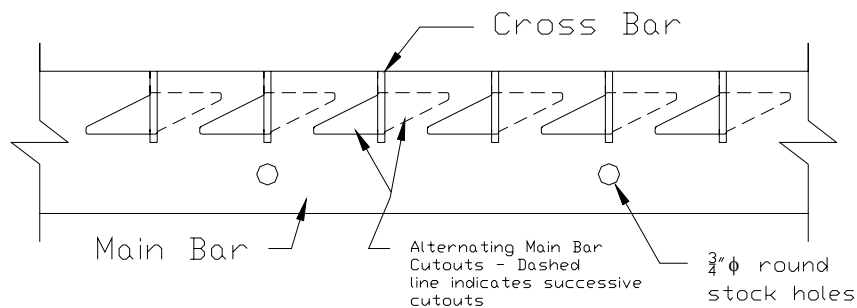


**Figure 3.2 - Deck Elevation**  
**(Dashed lines indicate successive alternating cutouts)**

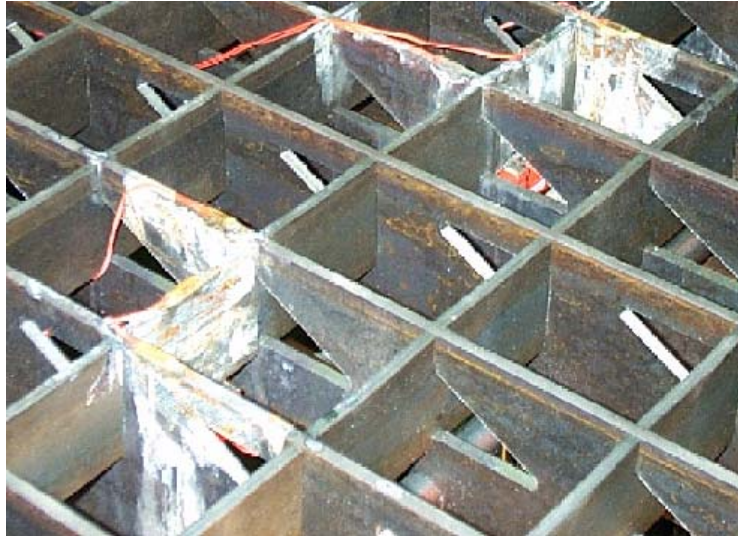


**Figure 3.3 - Alternating Main Bar Cutouts**

### **3.2 MANUFACTURING TECHNIQUE**

A novel characteristic of this weldless deck system is its efficient manufacturing technique. The structural integrity of the weldless deck is a function of the mechanical interference developed between the main bars and cross bars during fabrication. A patented assembly process (Imm, 2000 – Patent Number 6,018,833) involves the insertion of notched cross bars through alternating main bars cutouts. To do so, the main bars are staggered along their longitudinal axis in alternating positions [Figure 3.4] to create a clear insertion aperture through the cutouts.

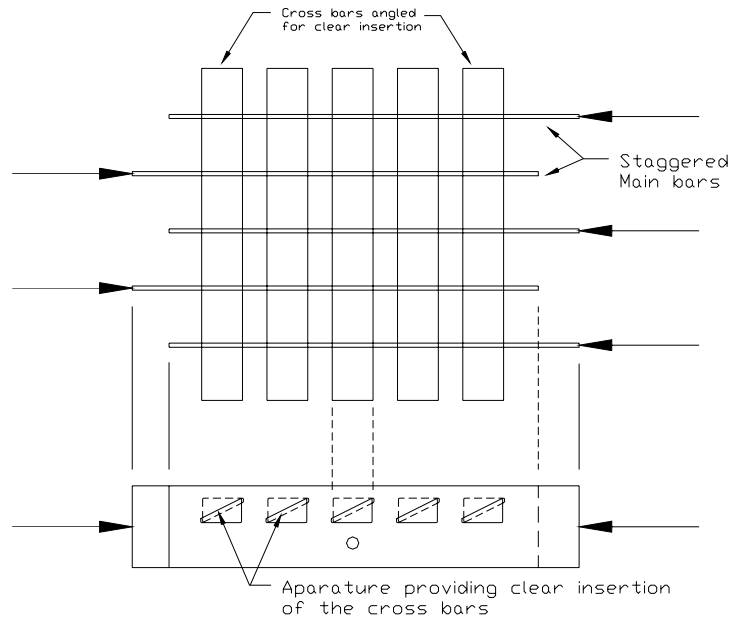


**Figure 3.4 - Assembly Process**

Upon complete insertion of the cross bars, the main bars are forced together in a hydraulic press to bring the bar ends into coincidence and hence square the deck (indicated by the arrows in Figure 3.4). Due to machining tolerances, mechanical interference is developed between main bars and cross bars and hence the structural integrity is further enhanced. The deck is finally secured by way of locking pins inserted at the locations described in Section 3.1.

## 4.0 LABORATORY PROCEDURES

### 4.1 DESCRIPTION OF LOAD FRAME AND ACTUATORS

The present research program was carried out in the Watkins-Haggart Structural Engineering Laboratory at the University of Pittsburgh. The facility contains a 15-ton stand-alone testing frame mounted atop a two-foot thick concrete reaction floor. The frame is an assembly of multiple steel components including two (2) 5-ton, stiffened base beams which support two box beams topped with knife edges to provide simple supports for the deck. A third elevated box beam supported the actuators used to apply fatigue and ultimate strength loadings. The loading frame is illustrated in Figure 4.1. Additional laboratory photos can be found in Appendix B.

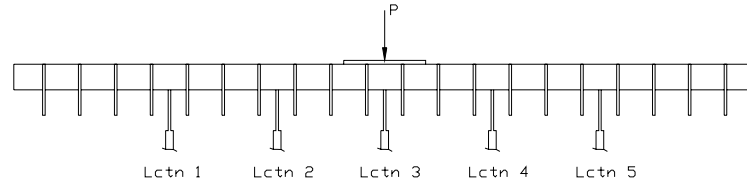


Figure 4.1 – Load Frame and Weldless Deck

Fatigue and ultimate loadings were applied using a closed-loop servo-hydraulic testing system with two different actuators. A 25 kip MTS actuator was employed during fatigue testing and a 250 kip actuator was used in performing the ultimate strength test. Two different hydraulic actuators were used in the testing program for efficiency. Since the fatigue testing program involved a peak load of only 13.8 kips, a smaller actuator was used thus reducing the demand for pumping capacity. Subsequently, a higher loading frequency was reached as compared with what could have been achieved using the 250 kip actuator. One of the laboratory's two (2) 60 GPM hydraulic power units provided the required pumping capacity necessary to execute the test.

## **4.2 INSTRUMENTATION**

The deck was tested as a simple span to produce maximum stress and deflection at midspan. As a result, detailed instrumentation was required at midspan to properly monitor the deck behavior. Thirty (30) independent foil strain gauges were applied to both the main and cross bars at top and bottom locations. A schematic of gauge locations is given in Appendix A. All gauges were placed with their longitudinal axis coinciding with the longitudinal axis of the given bar. The top Gauges TM7, TC8, and TM9 (location under the foot of actuator) were applied to the side of their respective bars,  $\frac{1}{4}$ " below the top of the bar to avoid direct contact with the foot of the actuator.



**Figure 4.2 - DCDT Elevation: Section shown at longitudinal mid span**

As shown in Figure 4.2, five Direct Current Displacement Transducers (DCDT) were placed evenly across the transverse width at the deck midspan. The geometric center of the deck did not coincide with a main bar, thus requiring the placement of the DCDT's on the cross bars [Figure 4.2]. Each DCDT location corresponded to strain gauge locations – ensuring precise deflection and extreme fiber strain measurements.

The foregoing instrumentation provided adequate data for monitoring main and cross bar neutral axes, measuring maximum deflections, and for determining overall deck stiffness and behavior.

### **4.3 DATA ACQUISITION**

The collection of data was done electronically using a 40 channel Micro Measurements System 5000 data acquisition system (see Appendix B for photo). The system consisted of a PC containing the Strain Smart software, a power source to excite the DCDT instrumentation, and two System 5000 Scanners. Each strain gauge was independently and directly wired to the data acquisition system. The DCDTs, however, required the construction of a circuit board to which each DCDT was wired and subsequently extended to the acquisition system. The circuit board was needed

since the System 5000 did not provide adequate power to excite all five DCDTs; hence an external 12-volt power supply was required.

## **5.0 LOADING PROTOCOL AND TESTING PROGRAM**

### **5.1 AASHTO LRFD SPECIFICATIONS**

In investigating the fatigue behavior of the weldless grid deck for bridge applications it was necessary to apply the 1998 AASHTO LRFD Specifications. Typical welded open steel grid decks contain fatigue-prone details including web punch-outs and bar intersection welds. Based on the specifications, and verified by Klippstein (1993) and Mangelsdorf (1996), such details can be considered a fatigue category C. Skroback (1999), of the University of Delaware, applied a finite element model and laboratory testing procedures to determine the fatigue resistance of two welded open grid decks. Skroback's testing indicated that AASHTO's fatigue category A best described the performance of the open grid deck specimens. As a result, and given the lack of welds at bar intersections, a fatigue category C can be considered a conservative characterization of the fatigue category of the current weldless grid deck.

AASHTO's fatigue category C (AASHTO Table 6.6.1.2.5-3) is schematically illustrated by the S-N (Stress range vs. Number of cycles) curve shown in Figure 5.1. As the applied stress range increases above 10 ksi the number of cycles required to reach failure decreases linearly from 5,000,000 cycles to zero cycles. However, as the curve demonstrates, the ordinate of 10 ksi and 5,000,000 cycles corresponds to the endurance limit beyond which an infinite fatigue life is expected. Hence a loading of the

deck that produces an extreme fiber stress range of 10 ksi, and applied for 5,000,000 cycles, suffices in demonstrating infinite fatigue life for the weldless grid deck.

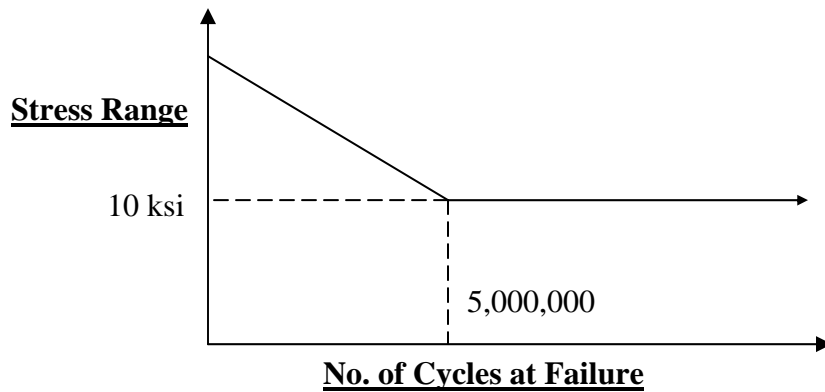


Figure 5.1 – S-N Curve

## 5.2 LOADING

### 5.2.1 Fatigue

With the requirements for fatigue set forth by the AASHTO Specifications, an equivalent suitably modified HS20 wheel load of 13.8 kips was applied to produce an extreme fiber stress of nearly 10 ksi (actual reading was 9.9 ksi). The 13.8 kip load was obtained from the application of a single HS20 tire patch service loading of 16 kips subsequently factored by 0.75 for fatigue and amplified by 15% for impact.

The load was applied using the 25 kip actuator with an 8" x 20" x 1" steel plate and neoprene pad simulating the effective contact area (patch size) of an HS20 truck tire. The patch size was determined in accordance with AASHTO 3.6.1.2.5. Loading

simulated a flow of traffic perpendicular to the longitudinal axis of the deck (the most common orientation in practice).

The fatigue testing program lasted for 20 days wherein 250,000 cycles of loading were applied to the deck each day, culminating with the completion of 5,000,000 cycles. Each cycle consisted of a sinusoidally varying load from 0.5 kips to 13.8 kips applied at a frequency of 10 Hertz. Rather than allowing the load to reach zero during cycling, a minimum load of 0.5 kips was instead maintained to stabilize the deck during testing (i.e. to keep the deck on the supports). Prior to the initial 250,000 cycles, a base-line response loading of 0 kips to 14 kips in 2 kip increments was conducted and the data recorded to establish a pre-fatigue benchmark deck response. Upon completion of each 250,000 cycles, a static test (identical to that of the base-line response test) was carried out providing insight into any change in structural performance of the weldless deck.

### **5.2.2 Ultimate Strength**

The ultimate strength test commenced upon completion of the 5,000,000 cycles of fatigue loading. The test was intended to characterize the ultimate capacity of the weldless deck while exposing the existence of undetected fatigue cracks. The 25 kip actuator was replaced with the 250 kip actuator and a systems check was conducted. Unfortunately, during the systems check, a control failure resulted in the actuator going to full-stroke and failing the deck. Although instrumentation was attached and excited, the data acquisition system was not active and hence did not record the data.

## **6.0 RESULTS AND DISCUSSION**

### **6.1 FATIGUE TESTING**

The results of the fatigue test were imported into Microsoft Excel and broken down accordingly. The raw form of the data output has been omitted, however, a formatted version is provided in Appendix C. Note that throughout testing a few gauges were lost and the DCDT at Location (Lctn) 2 malfunctioned. Exploiting symmetry, data for the DCDT at location 2 was replaced with that of the DCDT at Location 4.

#### **6.1.1 Stiffness Characteristics**

Illustrated in Figure 6.1, the stiffness of each deck location (corresponding to the DCDT locations) was found by plotting the applied load versus measured deflection. The slope of the resulting line for each fatigue cycle demonstrates the stiffness for the given location. The location shown (geometric center - directly under the applied load) demonstrates a pre-fatigue response stiffness of 133.56 kip/in and a post-fatigue stiffness of 125.47 kip/in. This can be seen as a 6.1% loss in deck stiffness over 5,000,000 cycles of an equivalent HS20 wheel load. Results from all five DCDT locations on the deck are summarized in Table 6.1. Additional plots are provided in Appendix C.

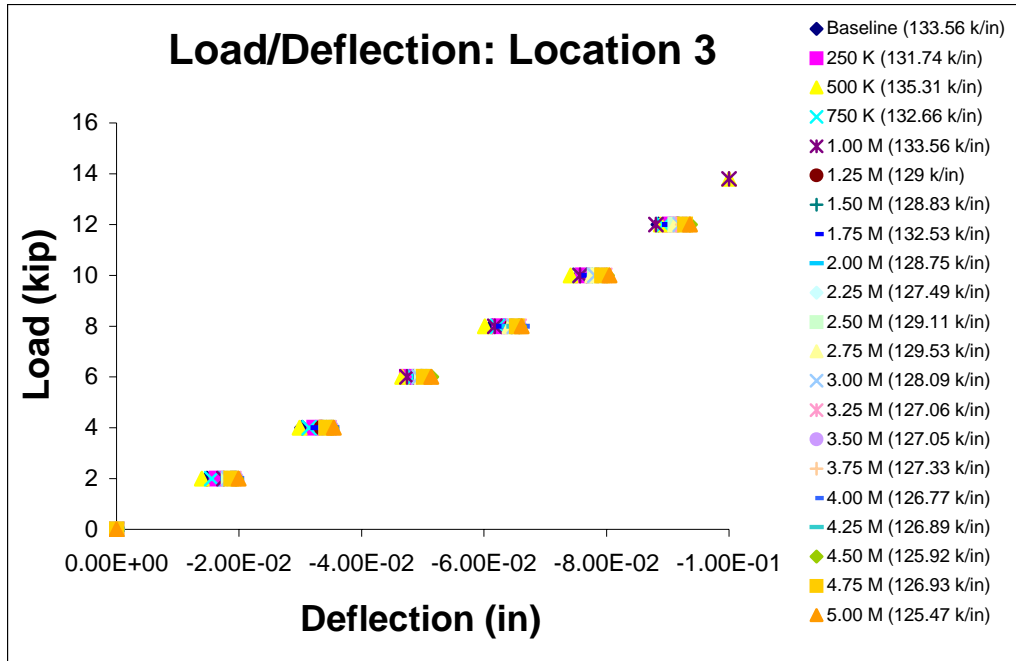


Figure 6.1 - Deck Stiffness: Location shown is deck center

Table 6.1 – Percent Change in Weldless Deck Stiffness  
(Stiffness units – kip/inch)

DCDT Location	Lctn 1	Lctn 2	Lctn 3	Lctn 4	Lctn 5
Pre-fatigue Response	205.43	161.27	133.56	161.27	228.27
Post-Fatigue (5M cycles)	198.39	153.39	125.47	153.39	206.35
<b>%Change</b>	3.4%	4.9%	6.1%	4.9%	9.6%

Location 3 demonstrated the lowest stiffness - as one may expect given this location was directly under the applied load. With the exception of location 5, the change in deck stiffness decreased in the transverse direction across the deck from the point of load application to edge of the deck. This suggests that, while the main bars

carried load in a longitudinal direction, the cross bars participated in distributing the load in a transverse direction and provided considerable deck stiffness.

An investigation of the data produced by the strain gauges reinforces the notion that the cross bars were participating in overall deck behavior. A plot of depth vs. strain for each load increment demonstrates the location of the neutral axis for pre- and post-fatigue. Figure 6.2 illustrates the position of the neutral axis for gauge locations TM6-BM25 and TC5-BC26 (corresponding to location 2 above) for pre- and post-fatigue.

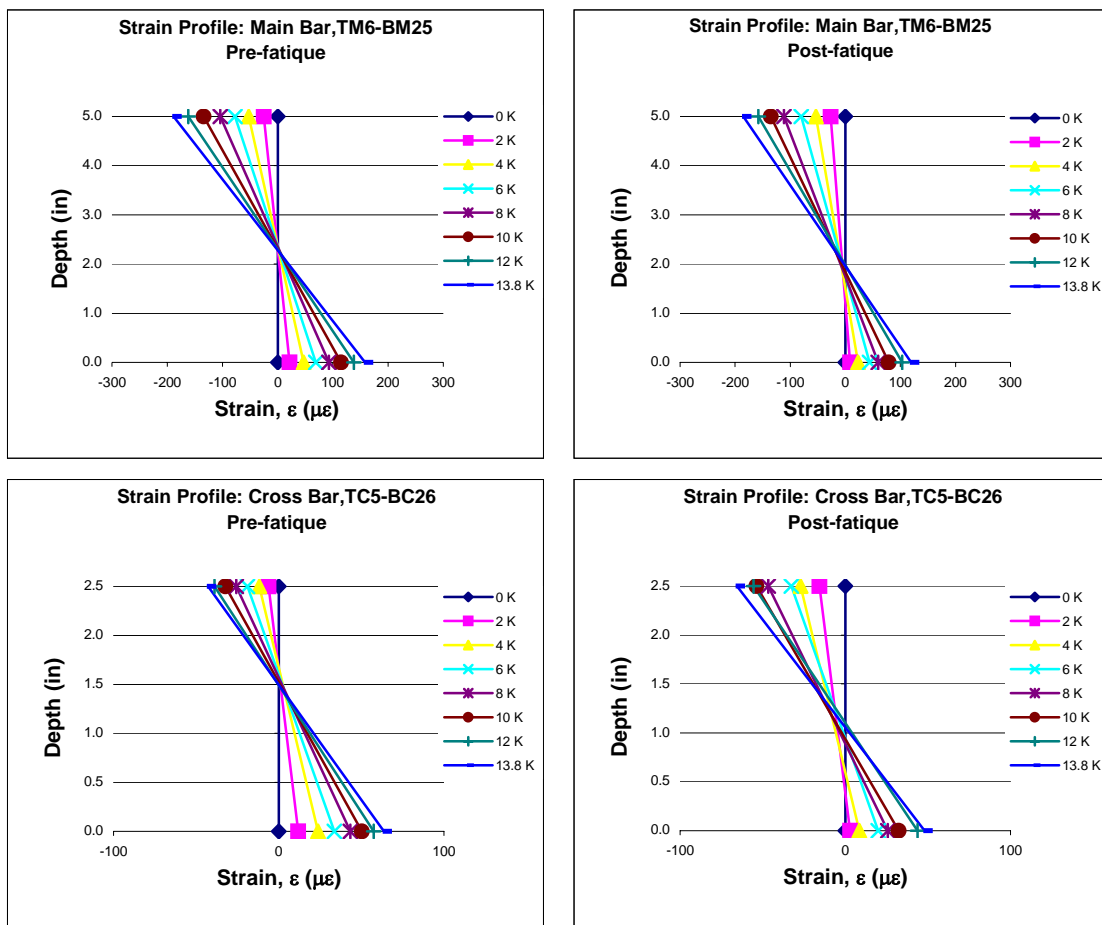


Figure 6.2 – Neutral Axis Locations

The main bar demonstrates a pre-fatigue neutral axis location at mid height (2.5"); this is approximately equal to that of the theoretical axis for a rectangular, prismatic member of one-half the depth. As the deck was fatigued, however, the strain in the compression zone (top) increased while the tensile strain (bottom) decreased, resulting in a small downward shift of the neutral axis. A similar behavior was observed in the relative position of the neutral axis of the cross bars. As the deck was subjected to fatigue loading, the cross bars participated in distributing the load throughout the deck and thus suffered a similar yet more dramatic change in neutral axis position. This suggests that while the cross bars significantly contributed to overall deck behavior, their stiffness was less than that of the main bars. Moreover, the longitudinal stiffness of the deck was greater than the transverse stiffness, demonstrating orthotropic behavior. As a result, and given the fact that no fatigue cracks were detected, the loss in deck stiffness can be attributed to the orthotropic behavior of the deck.

### **6.1.2 Deflection Profiles**

As expected, the maximum deflection was observed at midspan. The deflection profile of the deck is shown in Figure 6.3. The center of the deck experienced a pre-fatigue deflection of approximately 0.102" and a post-fatigue deflection of 0.106" at 13.8 kips. This demonstrates a change of only 4%. The greatest difference or change in the deflection profiles is the response of the deck at intermediate loads. As the load was increased, the post-fatigue deflection increased at a faster rate in comparison to pre-fatigue deflection. This indicates that after 5,000,000 cycles of loading, the cross bars

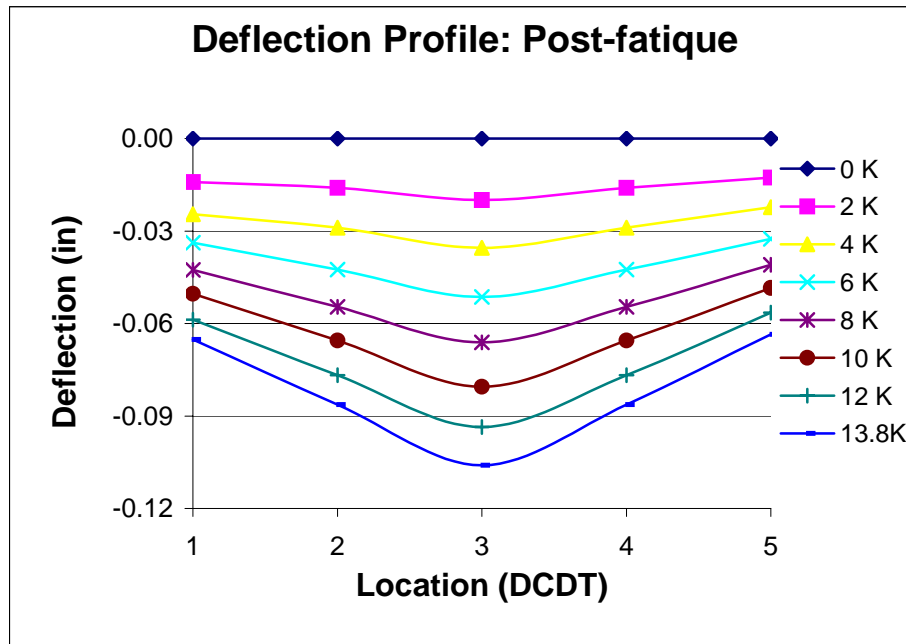
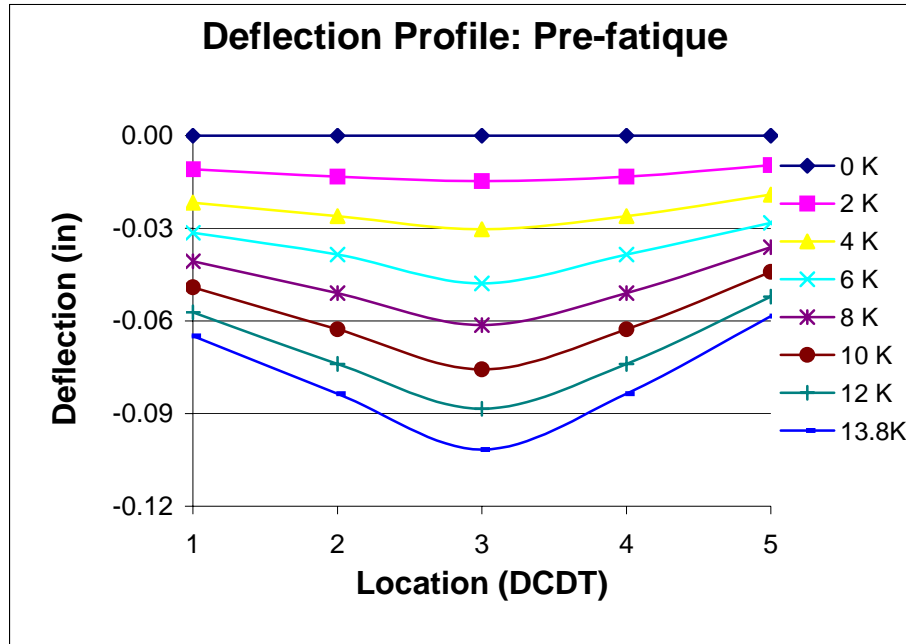
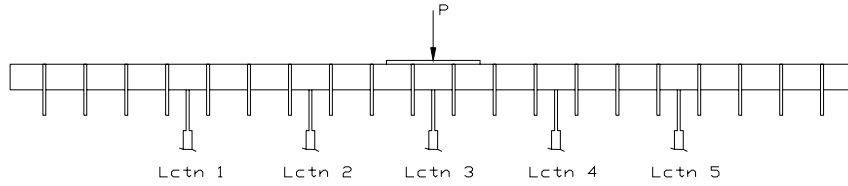


Figure 6.3 - Pre- and Post-fatigue Deflection Profiles  
Above figure shows DCDT locations

participated in resisting the lower static loads to a greater degree than they did the higher loads, while the main bars provided relatively constant stiffness. This is further reinforced with the greater change in cross bar strain behavior after the fatigue cycling.

Another observation is the change in shape of the deflection profile as the load increases. At lower loads, the profile is near linear suggesting the main and cross bars work together in resisting the load, and the cross bars distribute the load in a uniform fashion. However at higher load levels, the shape of the profile demonstrates a less uniform distribution of load in the lateral direction, particularly between Lctn 2 and 4. Comparing pre- and post-fatigue profiles show no change in the foregoing analysis.

## **6.2 ULTIMATE STRENGTH TESTING**

As a result of a controller failure the actuator unexpectedly went to full stroke and failed the deck. The actuator dead-ended with the deck having been subjected to deflections in excess of 6.0". Seen in Figure 6.4, the deck failed globally in a radial manner around the point of the applied load. At the load point, local buckling occurred in both the main and cross bars at a number of locations. Figure 6.4 shows buckling occurred in the main bars in an area about the cutouts while buckling of the cross bars was primarily observed directly under the load. A visual inspection of the severely distorted deck yielded no signs of fracture, which demonstrates the ductile nature of the weldless grid deck.

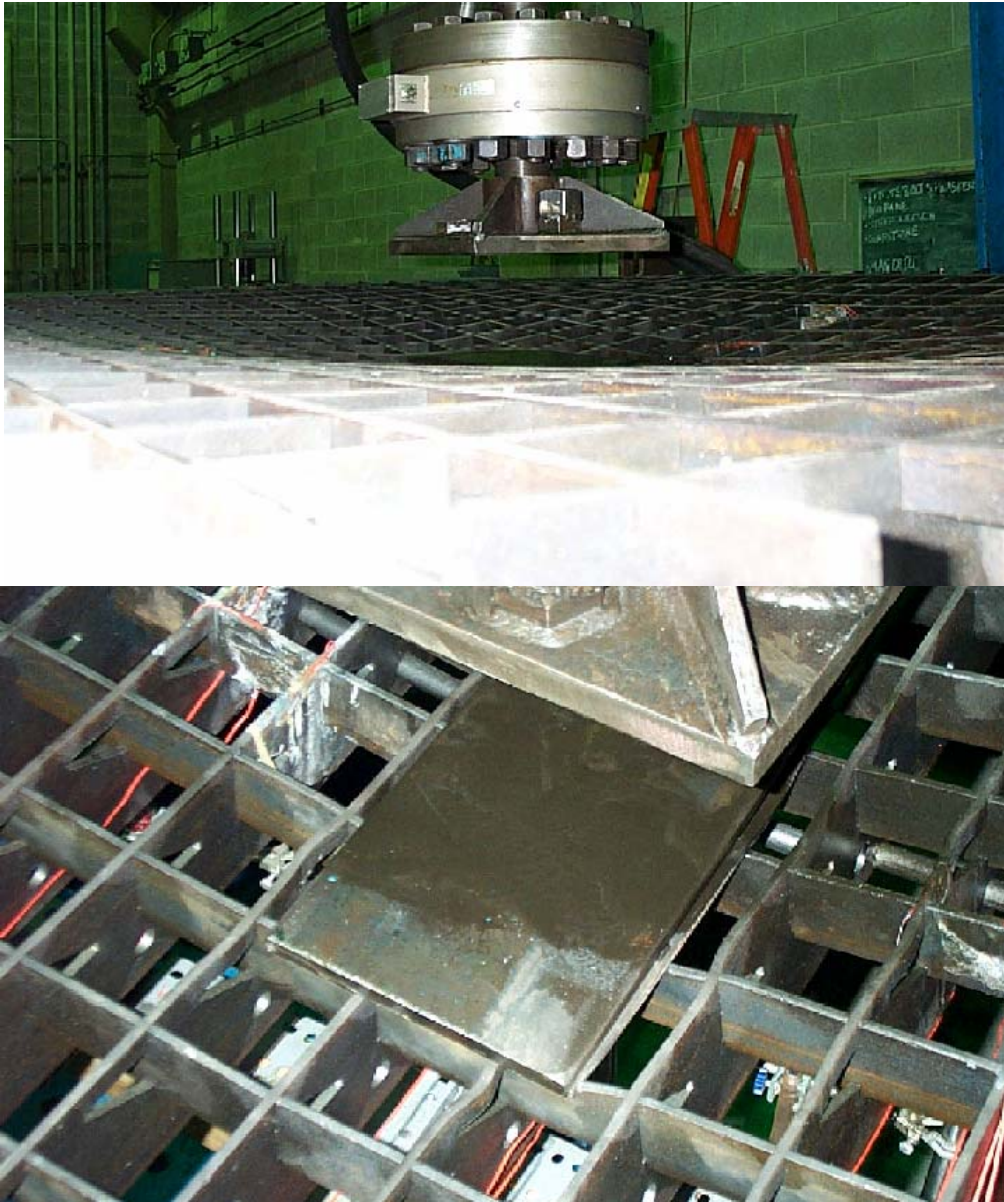


**Figure 6.4 - Weldless Grid Deck at Failure**

## **7.0 CONCLUSION**

### **7.1 FATIGUE TESTING**

The weldless deck manufactured by Stargrate Systems Inc. sustained 5,000,000 cycles of a suitably modified HS20 truck wheel load with little degradation in deck stiffness and strength. The applied load of 13.8 kips resulted in a maximum stress of 10 ksi, in accordance with AASHTO's fatigue category C (10 ksi stress range), and yielded a maximum stiffness loss of 10%. An analysis of the stiffness characteristics of the weldless deck showed significant participation of the cross bars in overall deck behavior. Given their smaller geometry, it is of no surprise there was a small loss in deck stiffness throughout 5,000,000 cycles of loading. The stiffness characteristics also demonstrate the orthotropic nature of the deck in exhibiting different properties in the two principle directions. This behavior is further illustrated by the deflection profiles of the weldless deck for both pre- and post-fatigue responses. As the deck responded to incremental loadings, the deflection illustrated a shift from a linear to a nonlinear transverse distribution of load. This indicates a change in the stiffness response of the deck, primarily in the transverse direction. In general however, a loss in deck stiffness of less than 10% is of little practical design importance.

## **7.2 ULTIMATE STRENGTH**

The ultimate strength test yielded a favorable performance of the weldless deck design. The deck demonstrated a very ductile mode of failure upon exceeding capacity and experiencing over 6.0" of deflection at the point of load application. The lack of fracture and fatigue cracks illustrates a ductile mode of failure and ensures a sudden failure will not occur.

## **7.3 RECOMMENDATIONS FOR FUTURE RESEARCH**

Further research may explore several avenues. A specimen can be tested in a continuous span condition to examine the effects of negative bending in both the longitudinal and transverse directions. Specimens of varying dimensions, steel properties or materials (i.e. aluminum, composite, etc.), can be tested for applications in different conditions. A final point of concern for investigation would be the need for the  $\frac{3}{4}$ " round stock locking pins fabricated with the weldless grid deck. Decks can be tested with the midspan locking pin continuous through the entire transverse width of the deck or without the locking pin in place. Further research may also focus on the need for such locking bars at the quarter points of the deck.

## **APPENDIX A**

### **STRAIN GAUGE LOCATIONS AND OVERALL GEOMETRY**

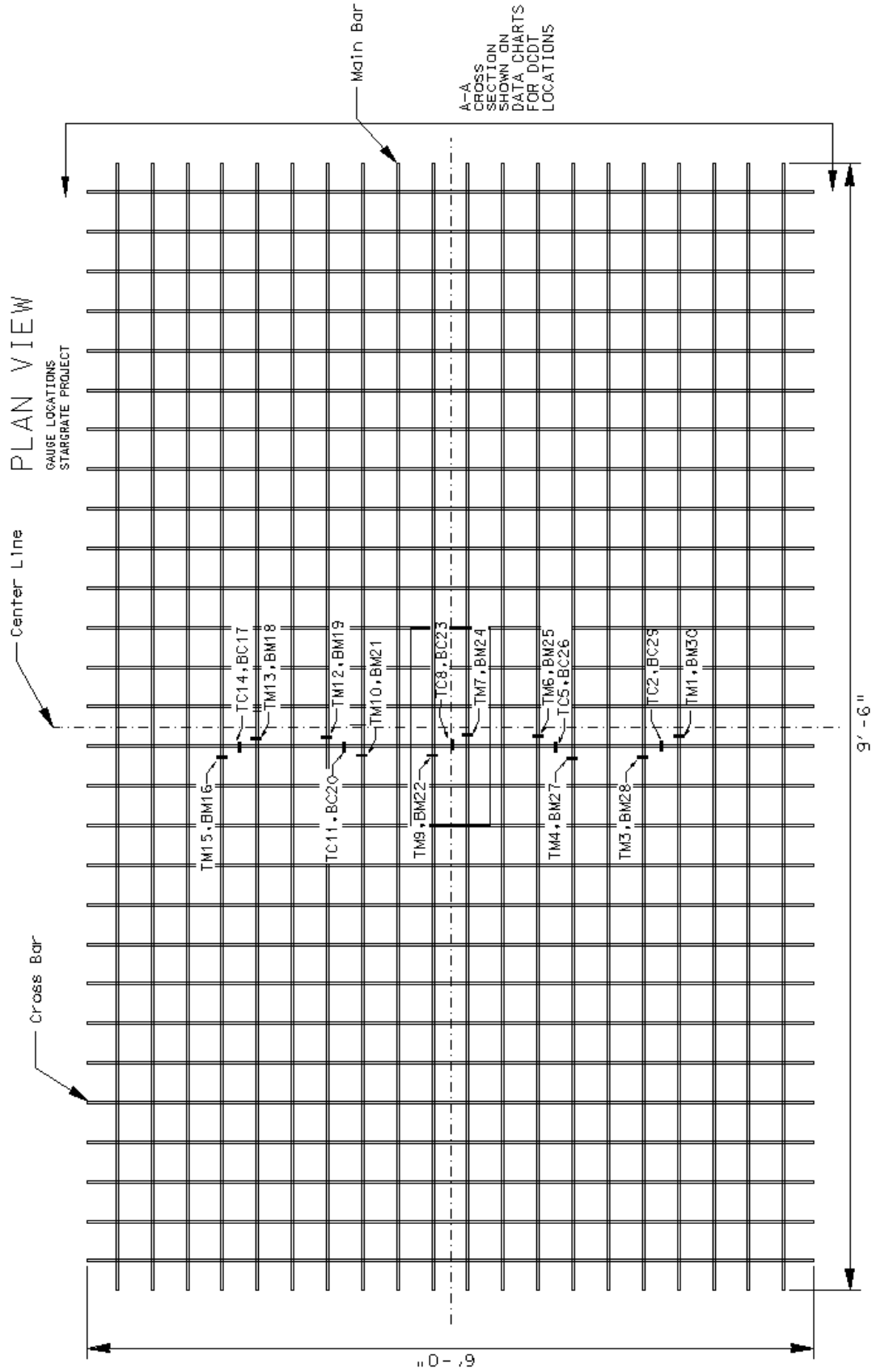
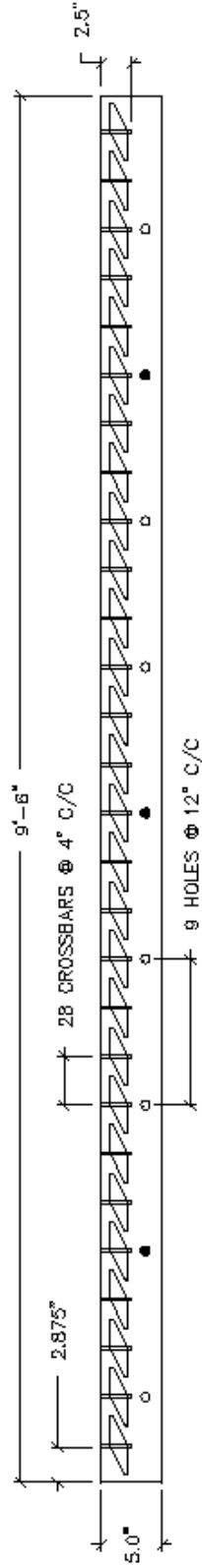


Figure A1 – Deck Plan View and Strain Gauge Location – Rectangle at center shows the placement of actuator foot  
 T – Top, B – Bottom, M – Main bar, C – Cross bar: Gauges numbered from bottom to top as shown



**Figure A2 – Deck Elevation - Filled holes indicate the location of the inserted round stock locking bars**  
**Note: only the midspan locking bar was present during testing**

**APPENDIX B**

**LABORATORY PHOTOGRAPHS**



**Figure B1 – MTS 458 Controller and Data Acquisition System**



**Figure B2 – DCDT Stand and Circuit Board**



**Figure B3 – 25 Kip Actuator Used in Fatigue Testing**



**Figure B4 – Foot of Actuator Used in Applying Load**



**Figure B5 – 250 Kip Actuator and Failed Weldless Grid Deck**



**Figure B6 – Transverse Deflection Profile**

## **APPENDIX C**

### **DATA BREAKDOWN AND ADDITIONAL RESULTS**

## STIFFNESS RESULTS

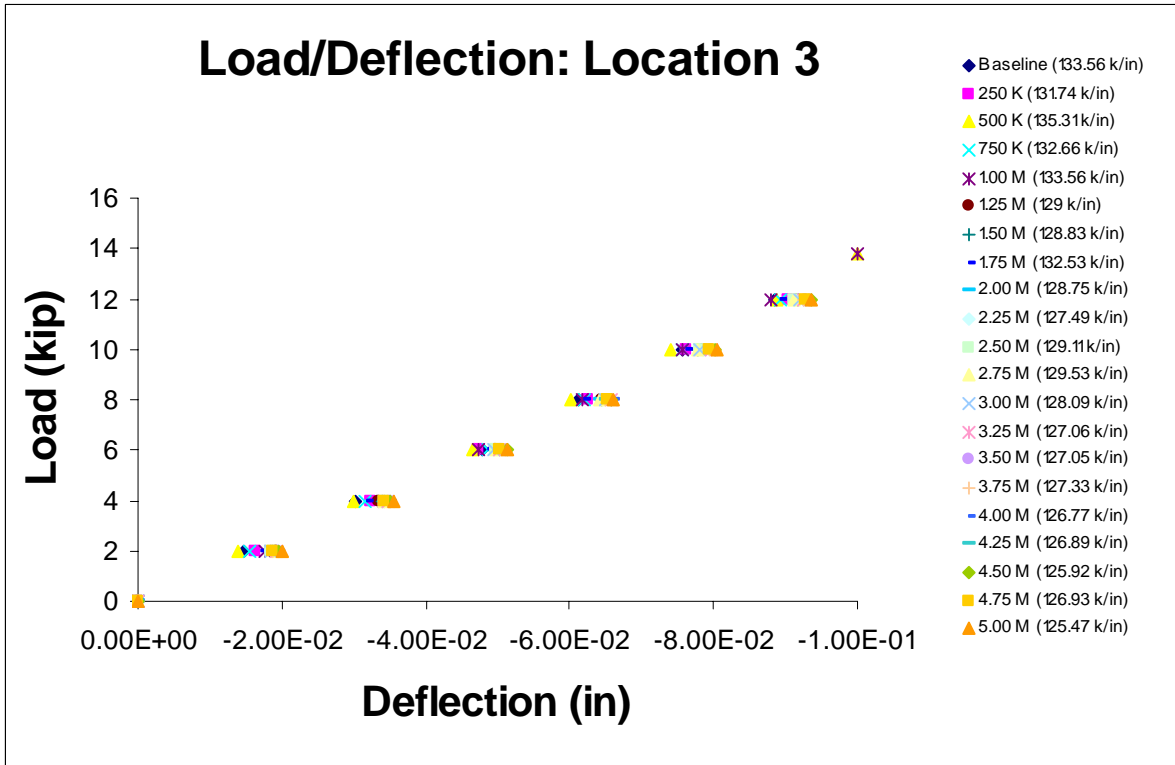
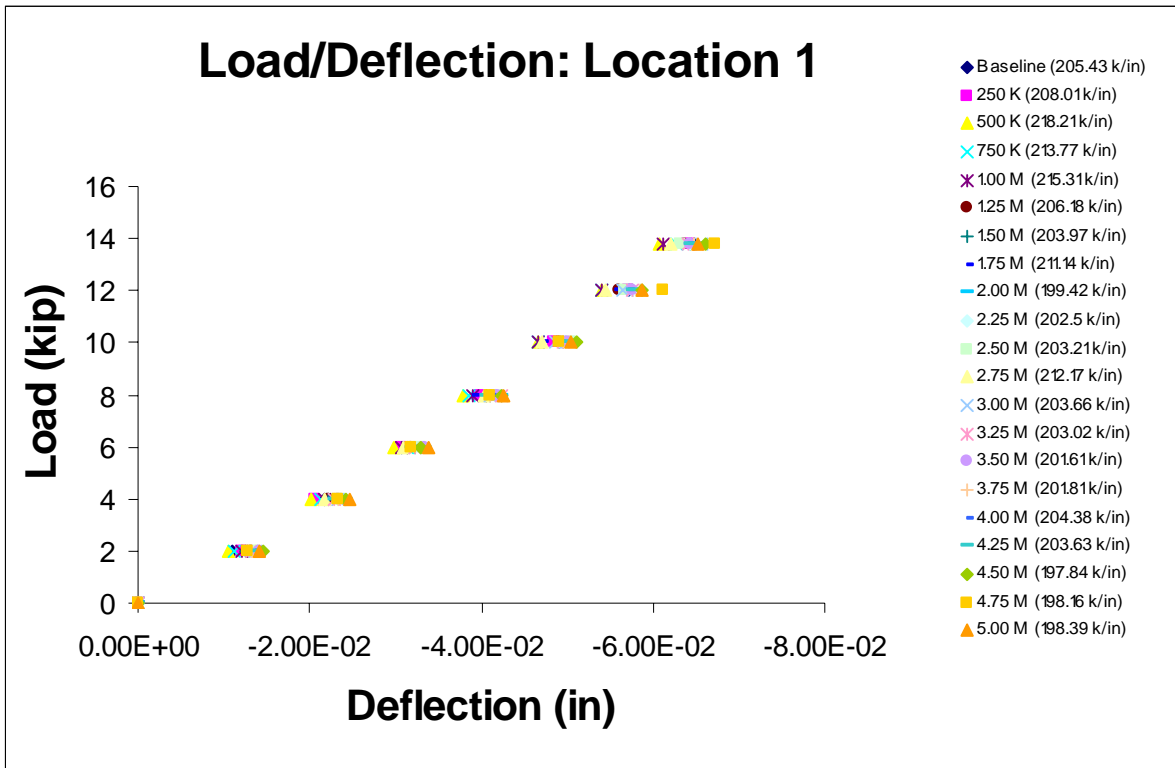


Figure C1 – Deck Stiffness Plots: Locations 1 and 3

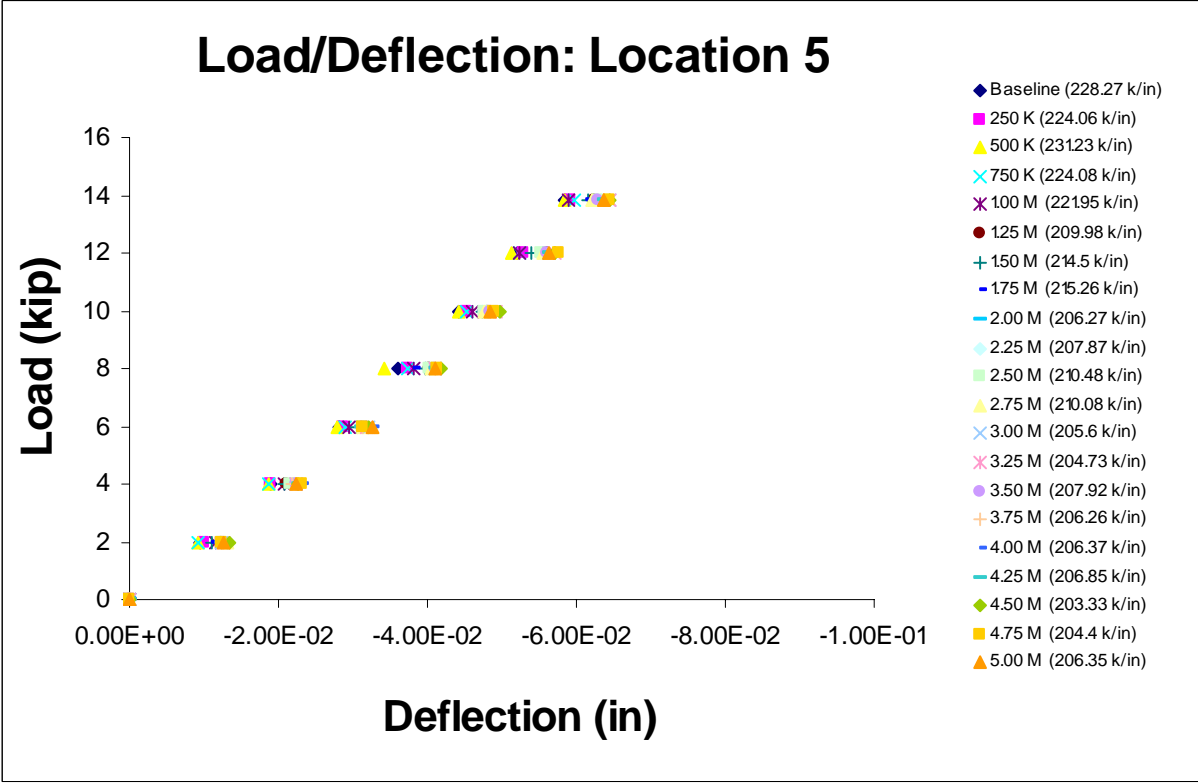
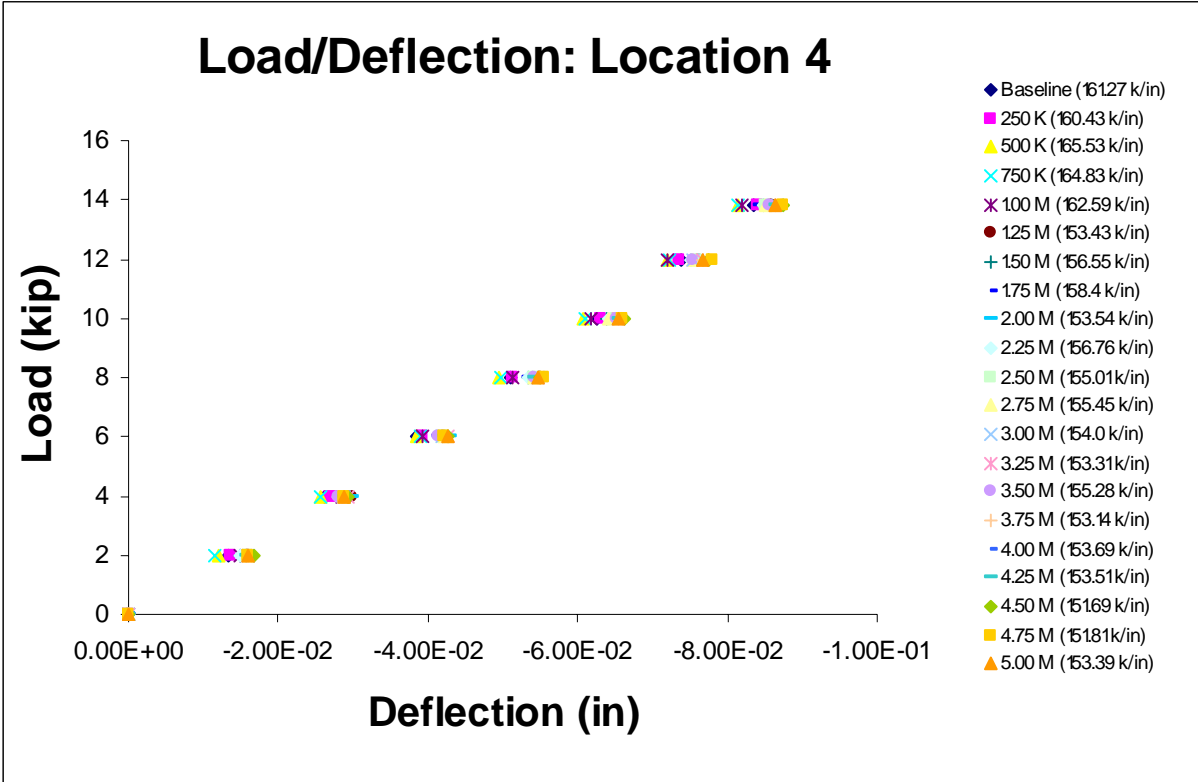


Figure C2 – Deck Stiffness Plots: Locations 4 and 5

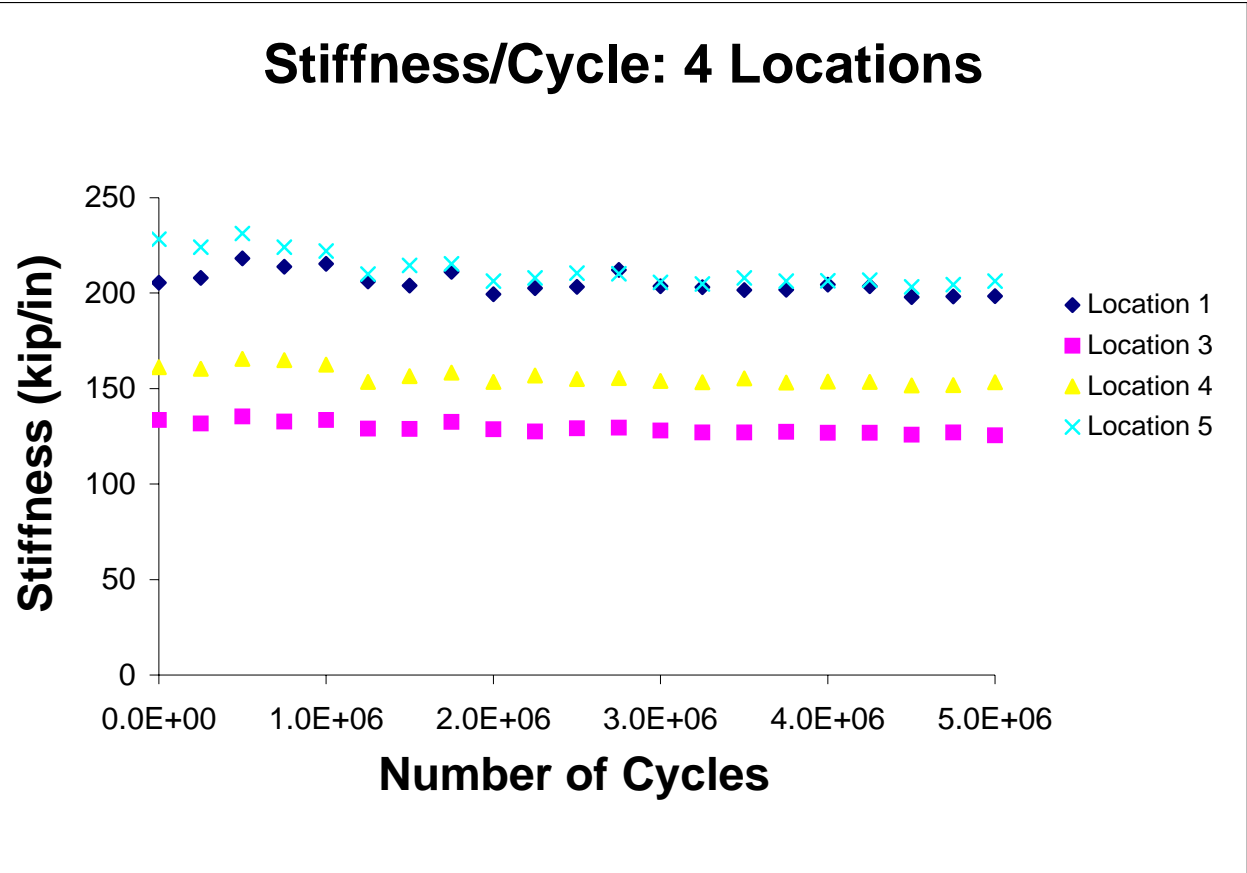


Figure C3 – Stiffness Per Number of Cycles

## DEFLECTION DATA

**Table C1 – Deflection Data**

<b>Pre-fatigue Deflections (in)</b>								
Load (kip)								
Location	0	2	4	6	8	10	12	13.8
1	0.0000	-0.0109	-0.0217	-0.0314	-0.0407	-0.0491	-0.0572	-0.0648
2	0.0000	-0.0133	-0.0261	-0.0386	-0.0510	-0.0626	-0.0739	-0.0835
3	0.0000	-0.0147	-0.0303	-0.0478	-0.0614	-0.0757	-0.0885	-0.1016
4	0.0000	-0.0133	-0.0261	-0.0386	-0.0510	-0.0626	-0.0739	-0.0835
5	0.0000	-0.0095	-0.0191	-0.0282	-0.0362	-0.0441	-0.0521	-0.0584

<b>Post-fatigue Deflections (in)</b>								
Load (kip)								
Location	0	2	4	6	8	10	12	13.8
1	0.0000	-0.0141	-0.0246	-0.0338	-0.0427	-0.0503	-0.0588	-0.0652
2	0.0000	-0.0161	-0.0289	-0.0426	-0.0546	-0.0655	-0.0767	-0.0863
3	0.0000	-0.0199	-0.0355	-0.0514	-0.0661	-0.0805	-0.0936	-0.1060
4	0.0000	-0.0161	-0.0289	-0.0426	-0.0546	-0.0655	-0.0767	-0.0863
5	0.0000	-0.0127	-0.0223	-0.0326	-0.0409	-0.0485	-0.0564	-0.0636

## MAIN BAR STRAIN GAUGE AND N.A. LOCATION DATA

**Table C2 – Pre-Fatigue Main Bar Strains  
(Gauges not shown indicate their data was unusable for the applicable analysis)**

Pre-Fatigue		Main Bars Strains (micro-strain)								
Main Bar Locations	Depth	Load (kips)								
		0	2	4	6	8	10	12	13.8	
TM	1	5	0.00E+00	7.06E+00	-1.36E+01	-2.59E+01	-6.59E+00	-1.41E+00	4.24E+00	8.94E+00
BM	30	0	0.00E+00	0.00E+00	0.00E+00	0.00E+00	0.00E+00	0.00E+00	0.00E+00	0.00E+00
TM	3	5	0.00E+00	-1.94E+01	-4.07E+01	-5.97E+01	-8.05E+01	-1.00E+02	-1.19E+02	-1.35E+02
BM	28	0	0.00E+00	2.06E+02	3.12E+02	5.11E+02	5.88E+02	6.71E+02	7.57E+02	8.44E+02
TM	4	5	0.00E+00	-2.32E+01	-4.83E+01	-7.29E+01	-9.89E+01	-1.25E+02	-1.49E+02	-1.73E+02
BM	27	0	0.00E+00	-3.16E+02	-9.07E+02	-1.43E+03	-8.55E+02	-1.71E+03	-1.41E+03	-1.86E+03
TM	6	5	0.00E+00	-2.52E+01	-5.23E+01	-7.70E+01	-1.04E+02	-1.34E+02	-1.62E+02	-1.88E+02
BM	25	0	0.00E+00	2.18E+01	4.70E+01	6.89E+01	9.31E+01	1.15E+02	1.38E+02	1.58E+02
TM	7	4.75	0.00E+00	-2.85E+01	-5.94E+01	-8.60E+01	-1.20E+02	-1.53E+02	-1.85E+02	-2.16E+02
TM	7	5	0.00E+00	-3.19E+01	-6.62E+01	-9.59E+01	-1.33E+02	-1.70E+02	-2.05E+02	-2.40E+02
BM	24	0	0.00E+00	3.55E+01	6.97E+01	1.03E+02	1.37E+02	1.71E+02	2.03E+02	2.34E+02
TM	9	4.75	0.00E+00	-2.18E+01	-4.69E+01	-7.15E+01	-1.00E+02	-1.31E+02	-1.60E+02	-1.88E+02
TM	9	5	0.00E+00	-2.43E+01	-5.23E+01	-7.98E+01	-1.12E+02	-1.46E+02	-1.77E+02	-2.09E+02
BM	22	0	0.00E+00	2.65E+01	5.63E+01	8.57E+01	1.16E+02	1.47E+02	1.79E+02	2.07E+02
TM	10	5	0.00E+00	-1.89E+01	-4.21E+01	-6.58E+01	-9.32E+01	-1.24E+02	-1.52E+02	-1.80E+02
BM	21	0	0.00E+00	1.85E+01	3.83E+01	5.91E+01	7.90E+01	9.98E+01	1.22E+02	1.41E+02
TM	12	5	0.00E+00	-1.28E+01	-2.56E+01	-3.92E+01	-5.35E+01	-7.00E+01	-8.48E+01	-9.99E+01
BM	19	0	0.00E+00	9.83E+00	2.05E+01	3.18E+01	4.31E+01	5.35E+01	6.60E+01	7.61E+01
TM	13	5	0.00E+00	-1.29E+01	-2.72E+01	-4.05E+01	-5.62E+01	-7.48E+01	-9.00E+01	-1.05E+02
BM	18	0	0.00E+00	1.38E+01	2.71E+01	4.37E+01	5.65E+01	6.84E+01	8.36E+01	9.69E+01
TM	15	5	0.00E+00	-1.14E+01	-2.42E+01	-3.56E+01	-5.03E+01	-6.50E+01	-7.73E+01	-9.01E+01
BM	16	0	0.00E+00	1.33E+01	2.47E+01	4.08E+01	5.32E+01	6.27E+01	7.31E+01	8.50E+01

## MAIN BAR STRAIN GAUGE AND N.A. LOCATION DATA CONTINUED

**Table C3 – Post-Fatigue Main Bar Strains**  
**(Gauges not shown indicate their data was unusable for the applicable analysis)**

Post-Fatigue		Main Bars Strains (micro-strain)								
Main Bar Locations	Depth	Load (kips)								
		0	2	4	6	8	10	12	13.8	
TM	1	5	0.00E+00	-9.91E+00	-1.23E+01	-1.27E+01	-1.79E+01	-2.03E+01	-1.42E+01	-1.79E+01
BM	30	0	0.00E+00	0.00E+00	0.00E+00	0.00E+00	0.00E+00	0.00E+00	0.00E+00	0.00E+00
TM	3	5	0.00E+00	-2.56E+01	-4.83E+01	-6.87E+01	-9.24E+01	-1.12E+02	-1.27E+02	-1.46E+02
BM	28	0	0.00E+00	7.63E+00	1.81E+01	3.38E+01	4.38E+01	5.62E+01	7.24E+01	8.39E+01
TM	4	5	0.00E+00	-2.70E+01	-5.39E+01	-7.76E+01	-1.07E+02	-1.32E+02	-1.53E+02	-1.78E+02
BM	27	0	0.00E+00	0.00E+00	0.00E+00	0.00E+00	0.00E+00	0.00E+00	0.00E+00	0.00E+00
TM	6	5	0.00E+00	-2.66E+01	-5.32E+01	-7.98E+01	-1.12E+02	-1.35E+02	-1.58E+02	-1.85E+02
BM	25	0	0.00E+00	8.55E+00	2.33E+01	4.42E+01	5.98E+01	7.88E+01	1.03E+02	1.20E+02
TM	7	4.75	0.00E+00	-2.75E+01	-5.41E+01	-8.26E+01	-1.17E+02	-1.42E+02	-1.68E+02	-1.98E+02
TM	7	5	0.00E+00	-2.94E+01	-5.85E+01	-8.99E+01	-1.27E+02	-1.56E+02	-1.84E+02	-2.18E+02
BM	24	0	0.00E+00	8.53E+00	2.94E+01	5.59E+01	7.96E+01	1.08E+02	1.39E+02	1.66E+02
TM	9	4.75	0.00E+00	-3.17E+01	-5.92E+01	-8.05E+01	-1.07E+02	-1.32E+02	-1.53E+02	-1.80E+02
TM	9	5	0.00E+00	-3.37E+01	-6.35E+01	-8.72E+01	-1.17E+02	-1.44E+02	-1.67E+02	-1.98E+02
BM	22	0	0.00E+00	6.15E+00	2.32E+01	4.78E+01	7.01E+01	9.56E+01	1.25E+02	1.50E+02
TM	10	5	0.00E+00	-3.08E+01	-5.87E+01	-8.23E+01	-1.15E+02	-1.41E+02	-1.68E+02	-1.97E+02
BM	21	0	0.00E+00	6.15E+00	1.94E+01	3.83E+01	5.16E+01	7.24E+01	9.61E+01	1.16E+02
TM	12	5	0.00E+00	0.00E+00	0.00E+00	0.00E+00	0.00E+00	0.00E+00	0.00E+00	0.00E+00
BM	19	0	0.00E+00	0.00E+00	0.00E+00	0.00E+00	0.00E+00	0.00E+00	0.00E+00	0.00E+00
TM	13	5	0.00E+00	-2.57E+01	-4.57E+01	-6.19E+01	-8.29E+01	-1.01E+02	-1.11E+02	-1.28E+02
BM	18	0	0.00E+00	3.80E+00	1.19E+01	2.33E+01	3.18E+01	4.27E+01	6.22E+01	7.36E+01
TM	15	5	0.00E+00	-2.61E+01	-4.32E+01	-5.79E+01	-7.82E+01	-9.39E+01	-1.03E+02	-1.18E+02
BM	16	0	0.00E+00	4.27E+00	1.09E+01	2.18E+01	2.85E+01	3.85E+01	5.74E+01	6.60E+01

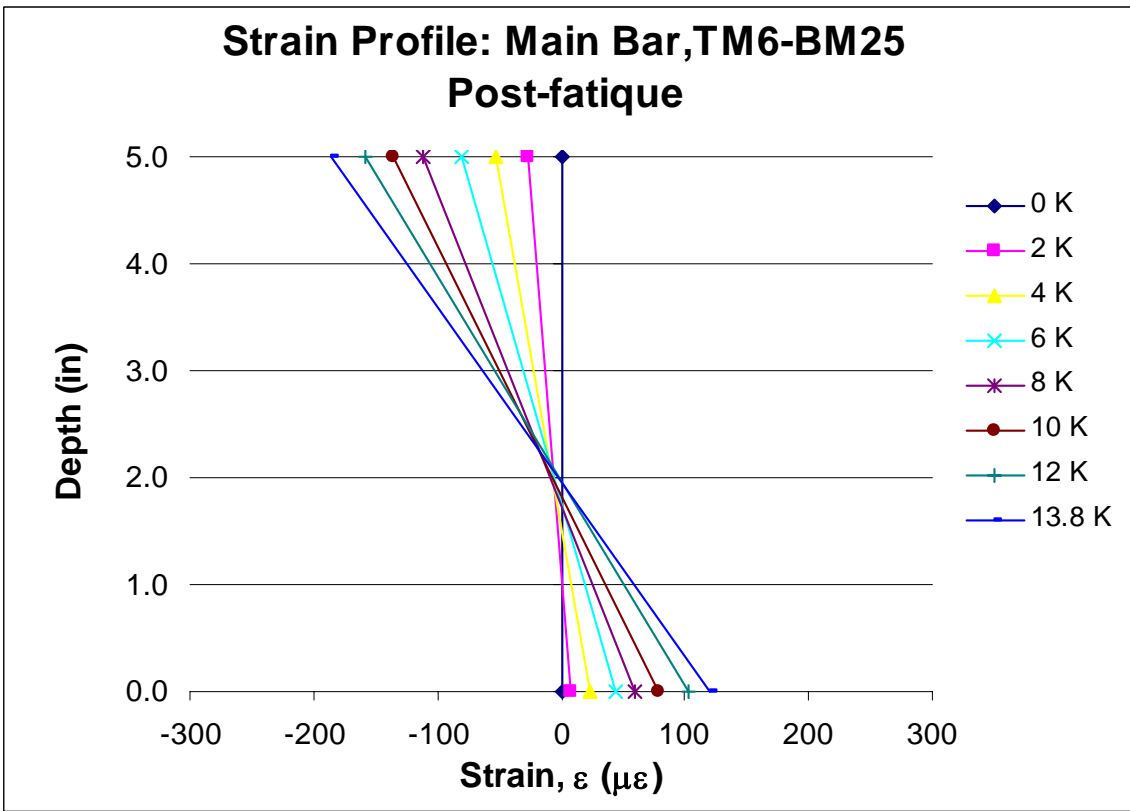
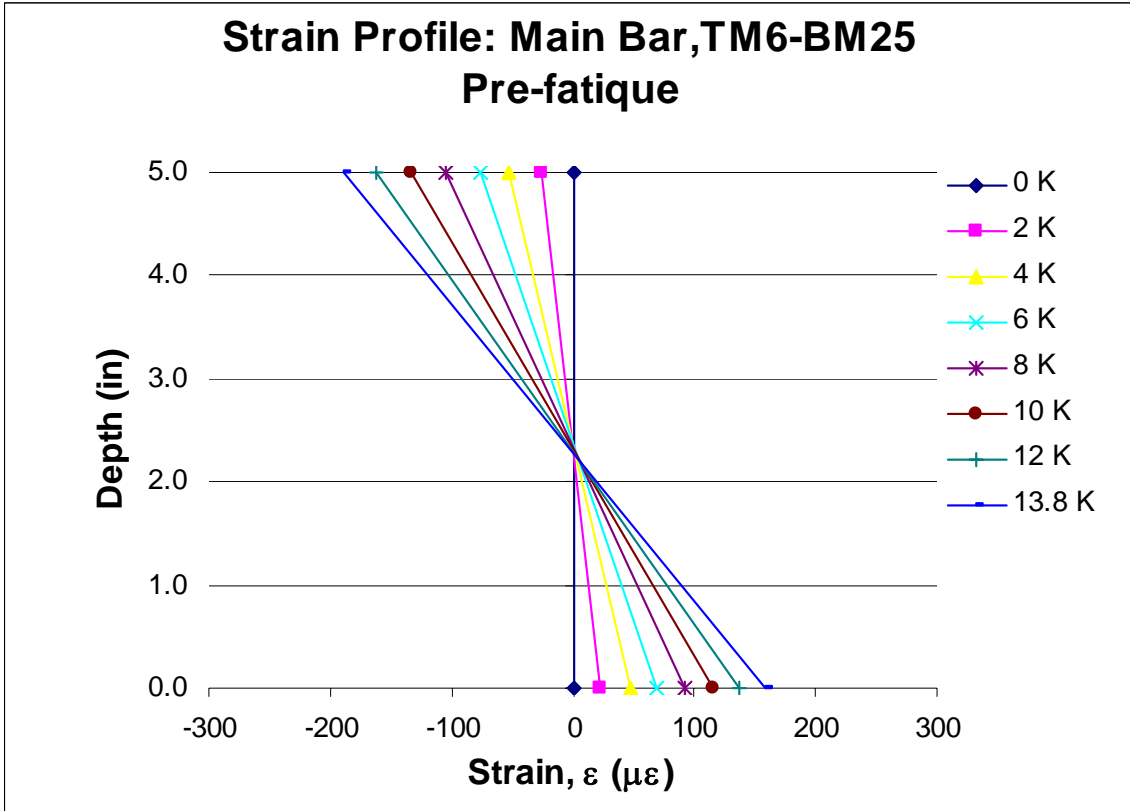


Figure C4 – Strain Profiles: Main Bar, TM6-BM25

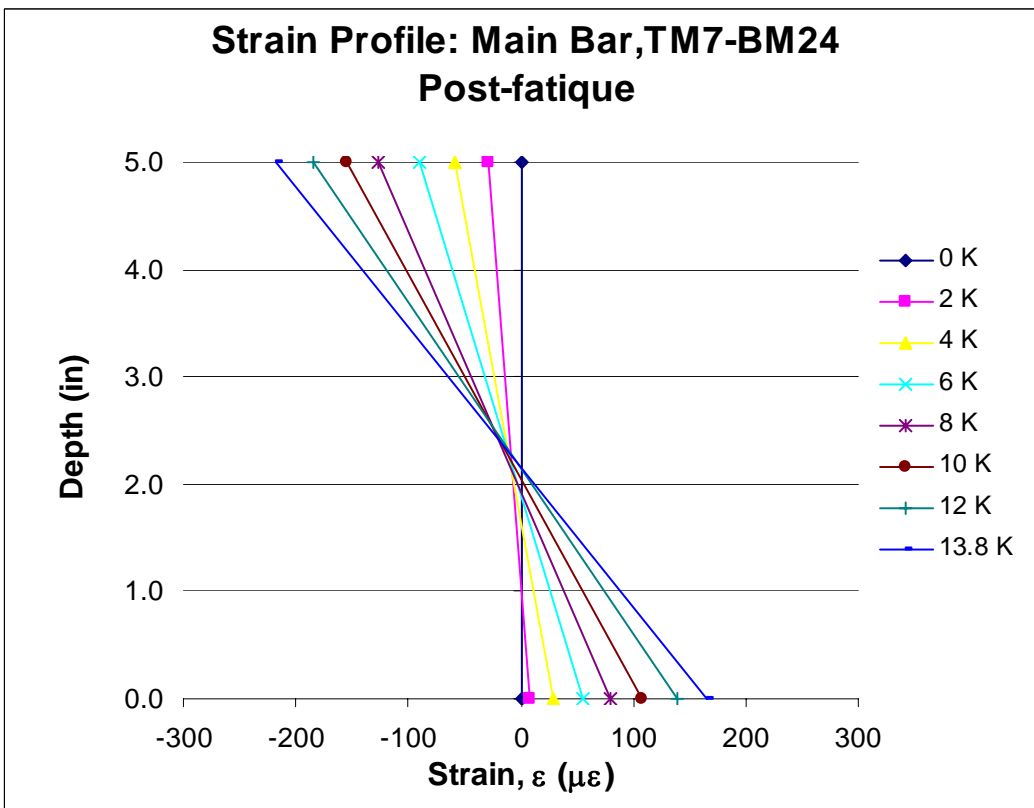
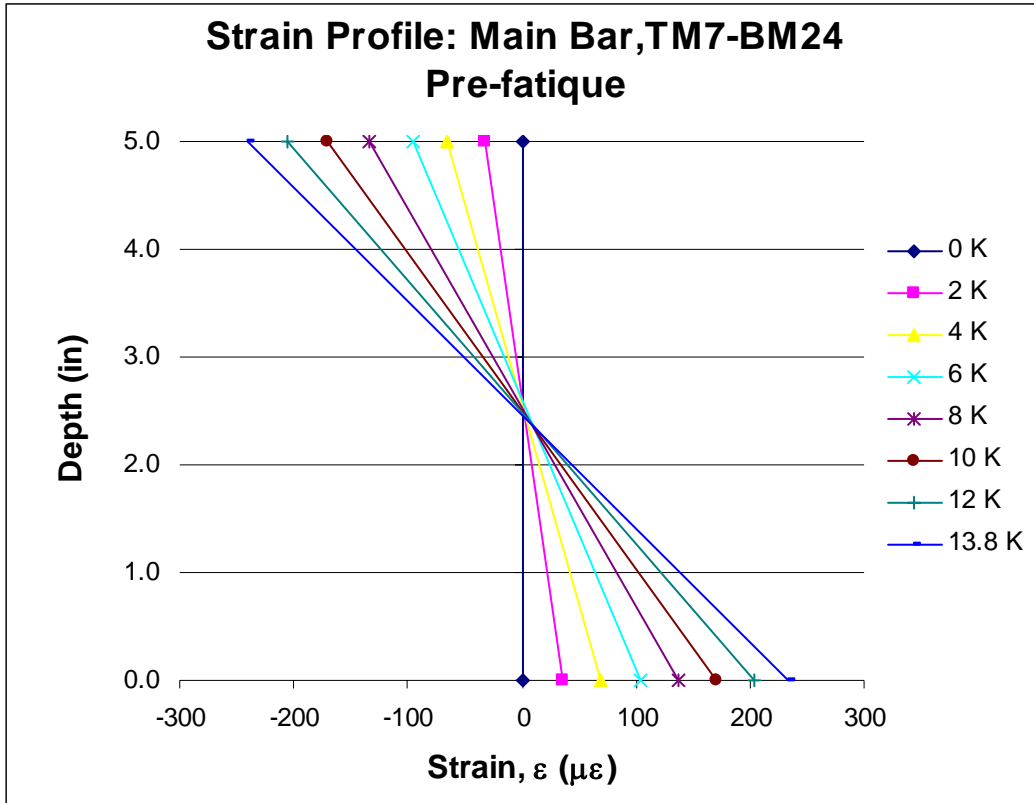


Figure C5 – Strain Profiles: Main Bar, TM7-BM24

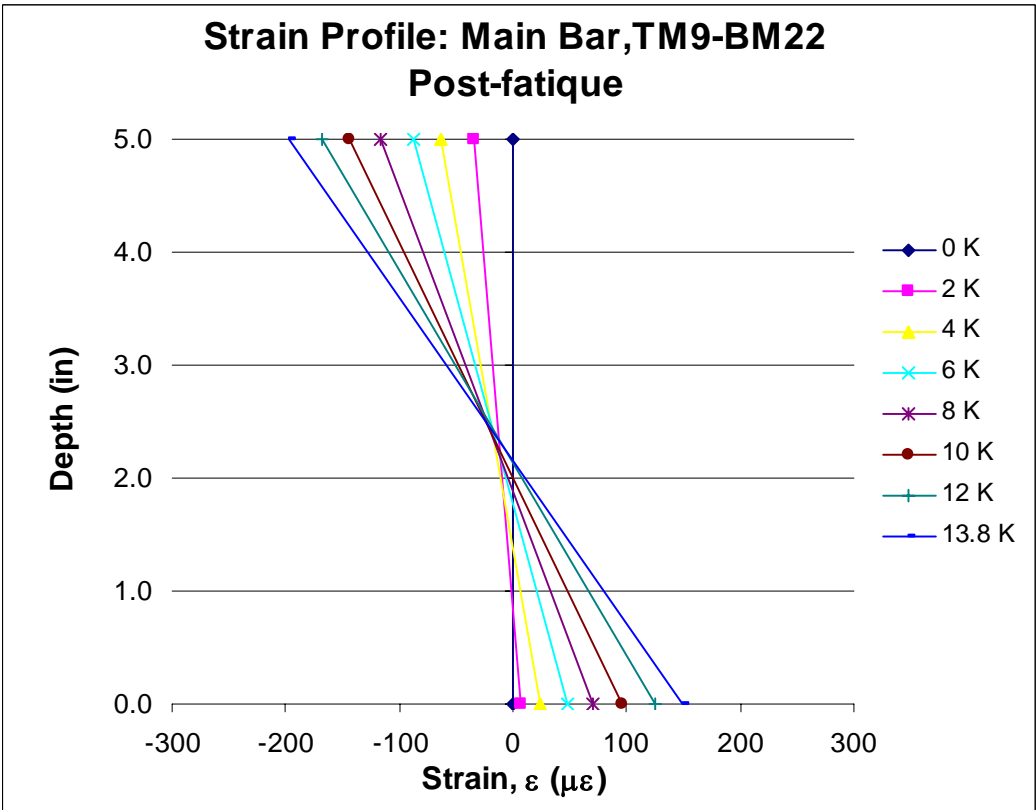
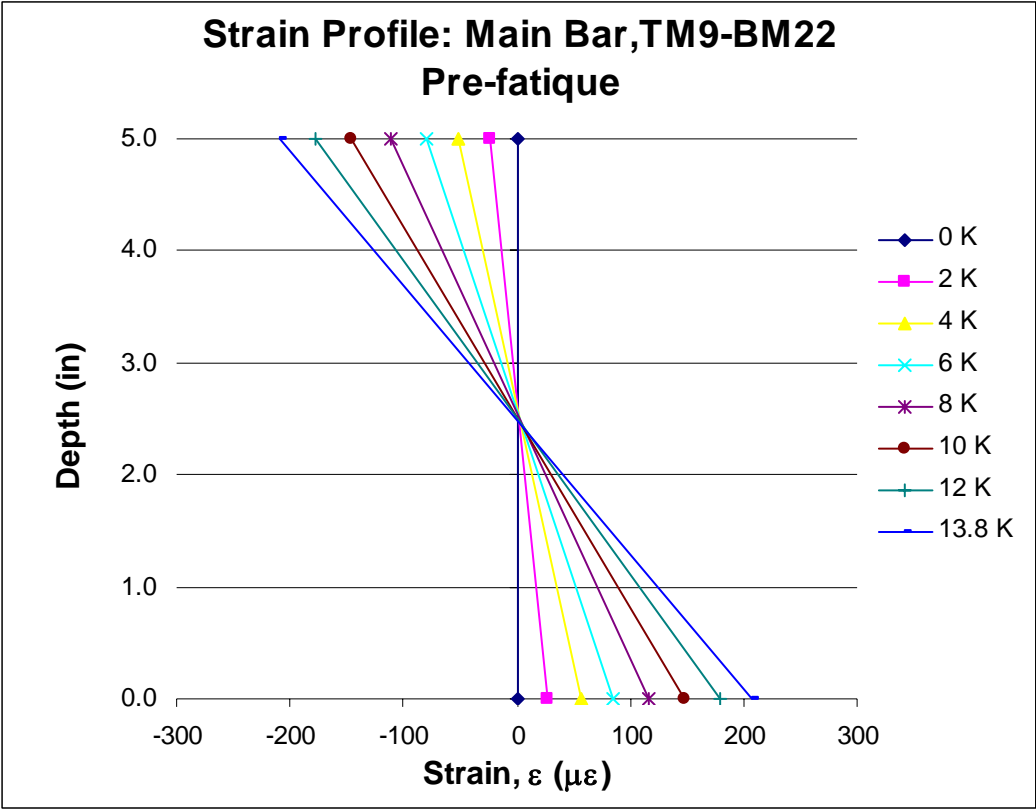


Figure C6 – Strain Profiles: Main Bar, TM9-BM22

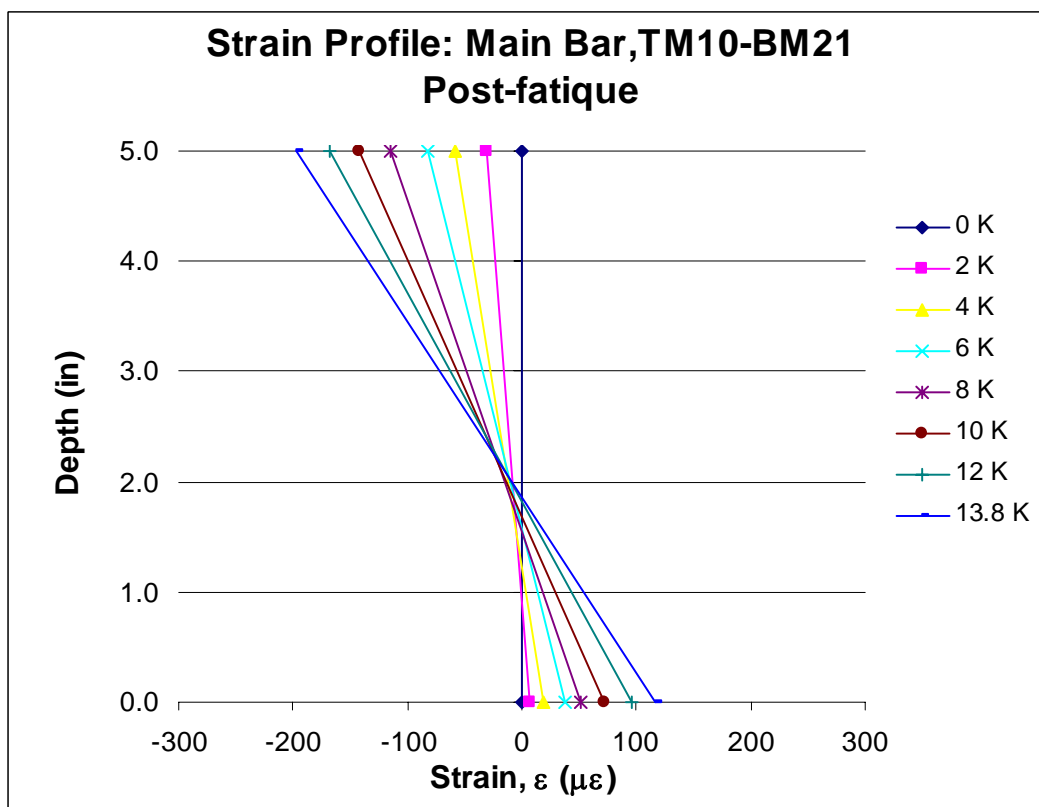
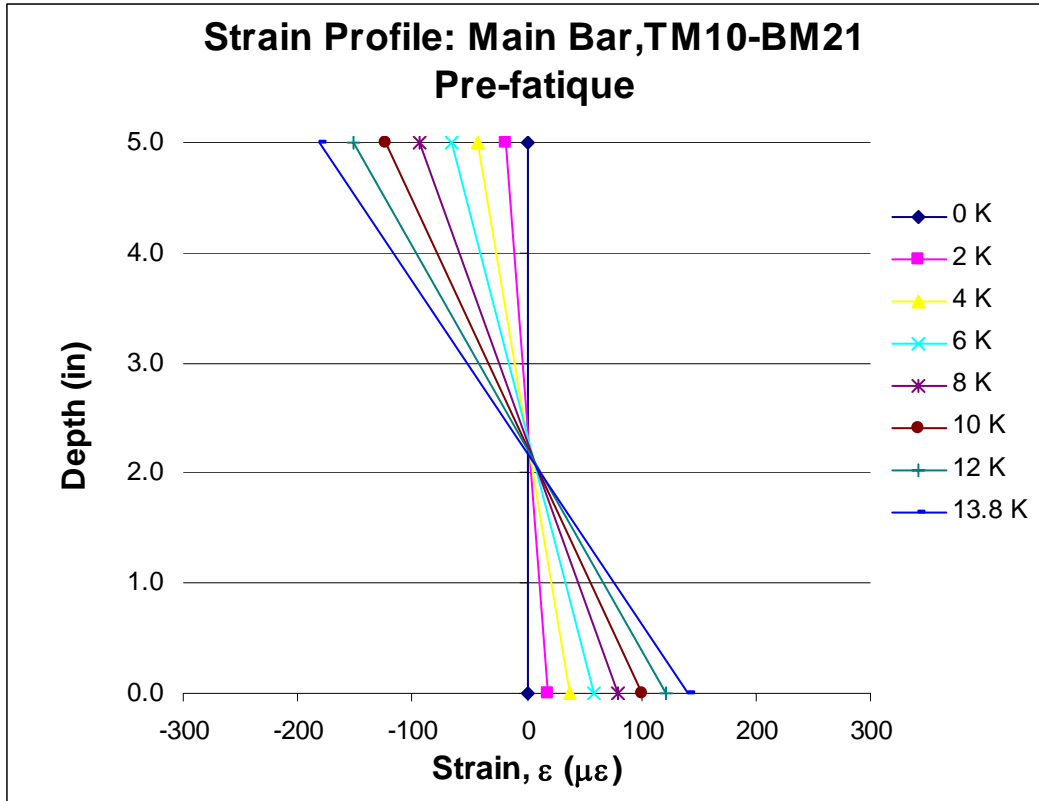


Figure C7 – Strain Profiles: Main Bar, TM10-BM21

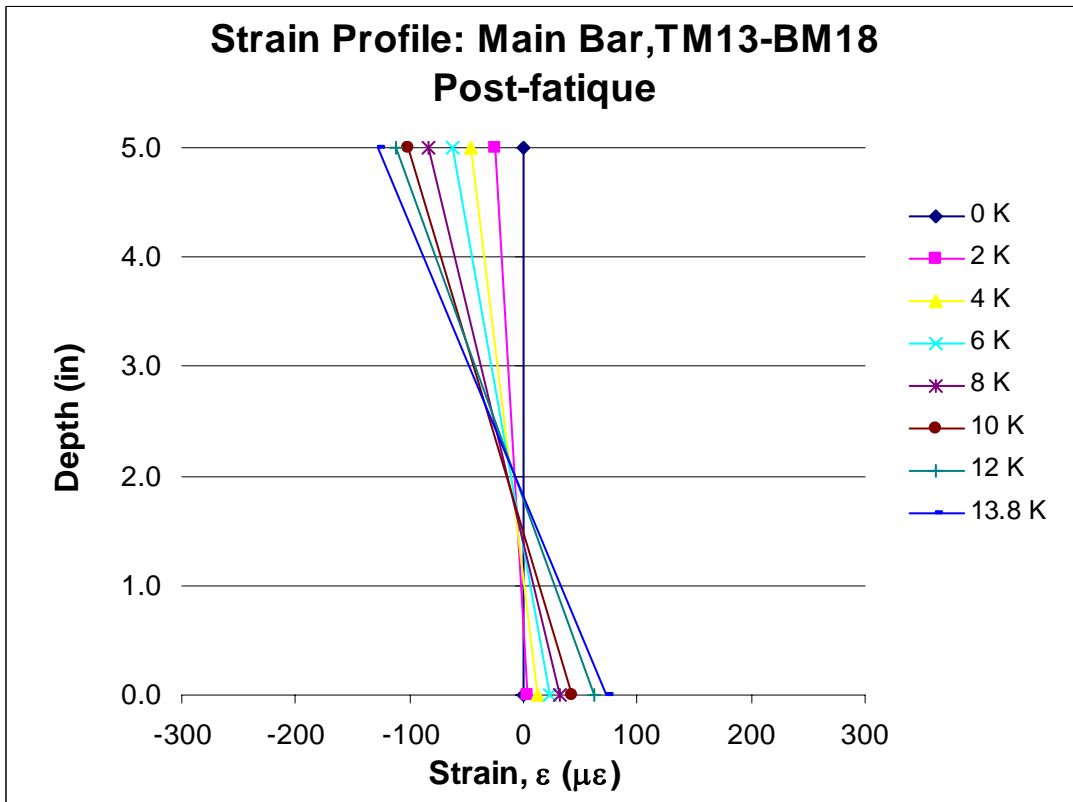
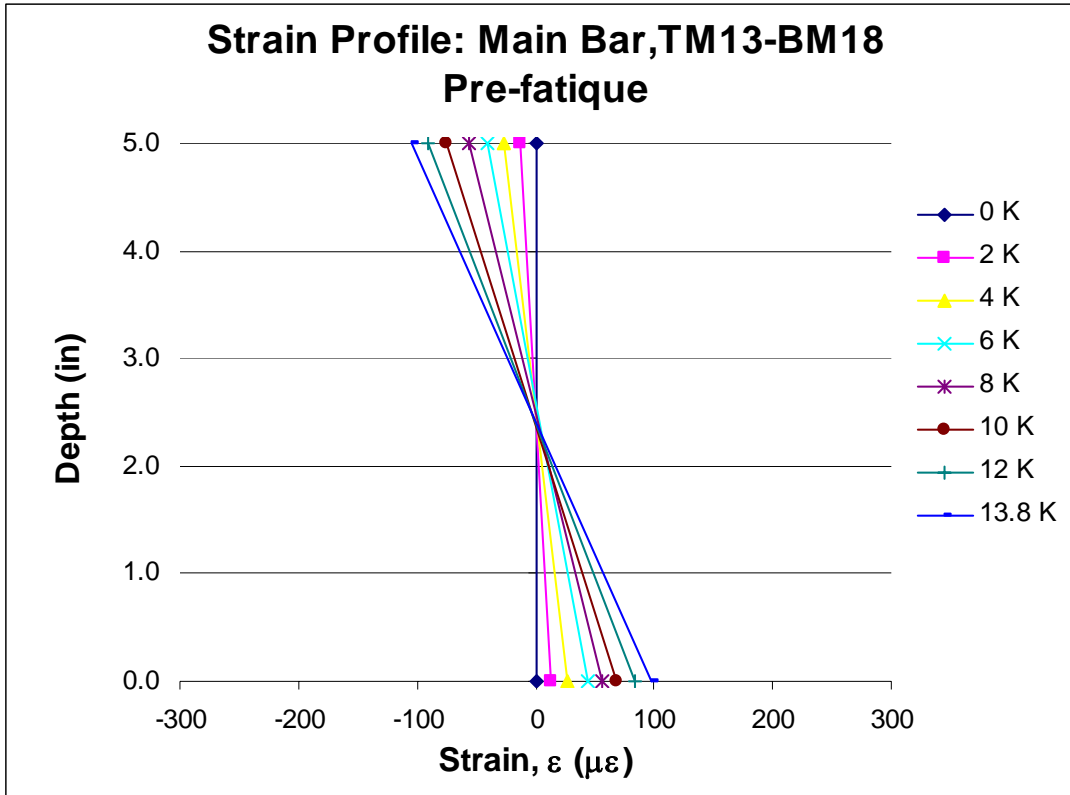


Figure C8 – Strain Profiles: Main Bar, TM13-BM18

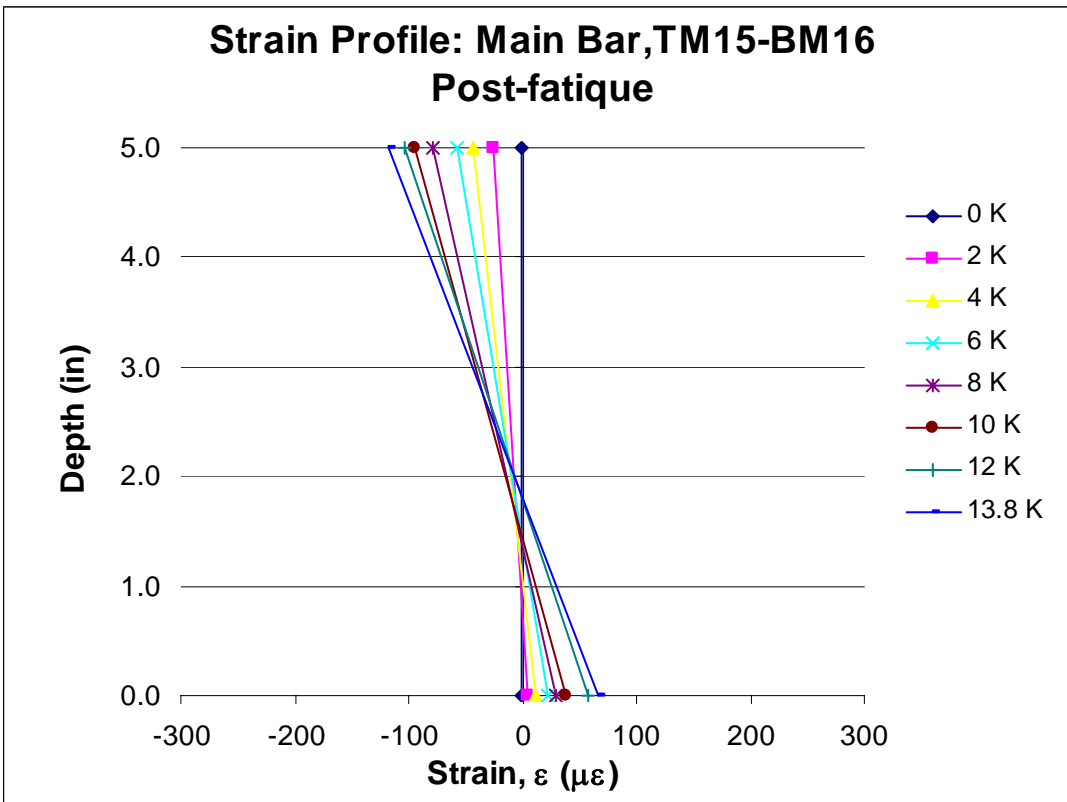
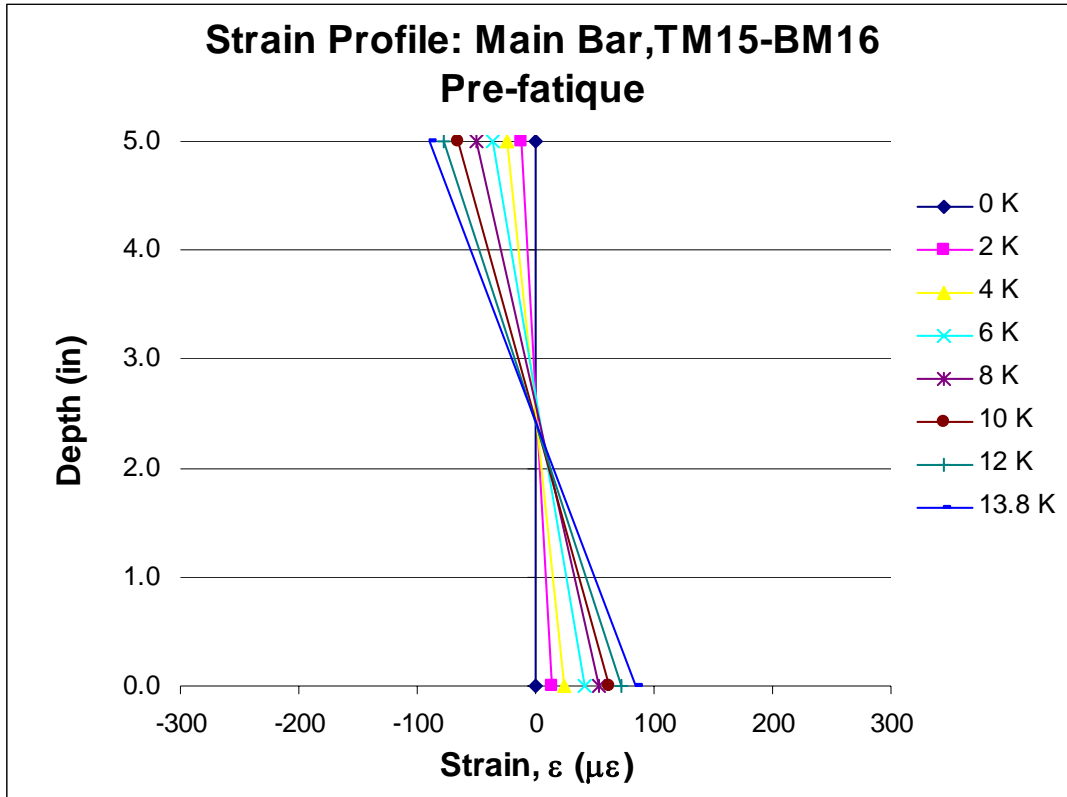


Figure C9 – Strain Profiles: Main Bar, TM15-BM16

**Table C4 – Main Bar Neutral Axis Data: TM6-BM25**

<u>Gauge</u> <u>TM6-BM25</u>	<b>Main Bar</b>		
	Pre-fatigue	Post-fatigue	Theoretical
Load	Location	Location	Location
0			2.5
2	2.3227	1.2158	2.5
4	2.3679	1.5213	2.5
6	2.3611	1.7811	2.5
8	2.3612	1.7448	2.5
10	2.3089	1.84	2.5
12	2.3014	1.976	2.5
13.8	2.2837	1.9624	2.5

**Table C5 – Main Bar Neutral Axis Data: TM7-BM24**

<u>Gauge</u> <u>TM7-BM24</u>	<b>Main Bar</b>		
	Pre-fatigue	Post-fatigue	Theoretical
Load	Location	Location	Location
0			2.5
2	2.6361	1.1228	2.5
4	2.5643	1.6705	2.5
6	2.5925	1.9166	2.5
8	2.5348	1.9248	2.5
10	2.5048	2.0432	2.5
12	2.4886	2.1523	2.5
13.8	2.4678	2.162	2.5

**Table C6 – Main Bar Neutral Axis Data: TM9-BM22**

<u>Gauge</u> <u>TM9-BM22</u>	<b>Main Bar</b>		
	Pre-fatigue	Post-fatigue	Theoretical
Load	Location	Location	Location
0			2.5
2	2.608	0.7719	2.5
4	2.5931	1.3378	2.5
6	2.5899	1.7705	2.5
8	2.5517	1.875	2.5
10	2.5128	1.9993	2.5
12	2.5086	2.1323	2.5
13.8	2.4922	2.154	2.5

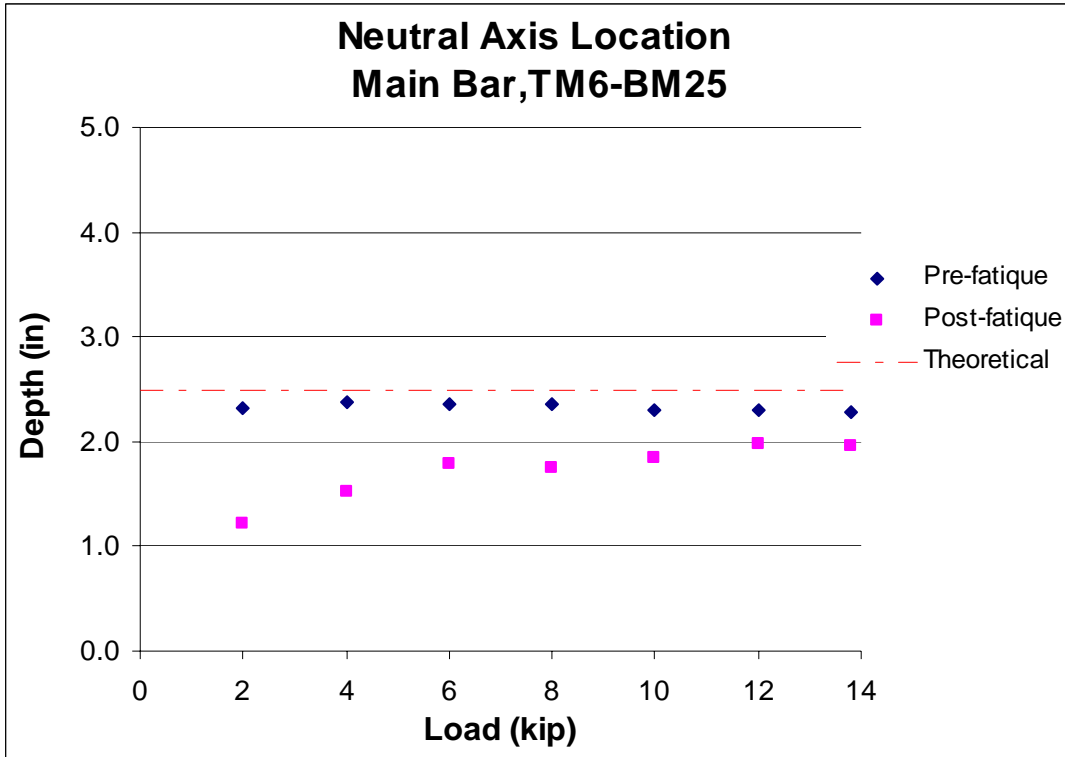


Figure C10 – Main Bar Neutral Axis Location: TM6-BM25

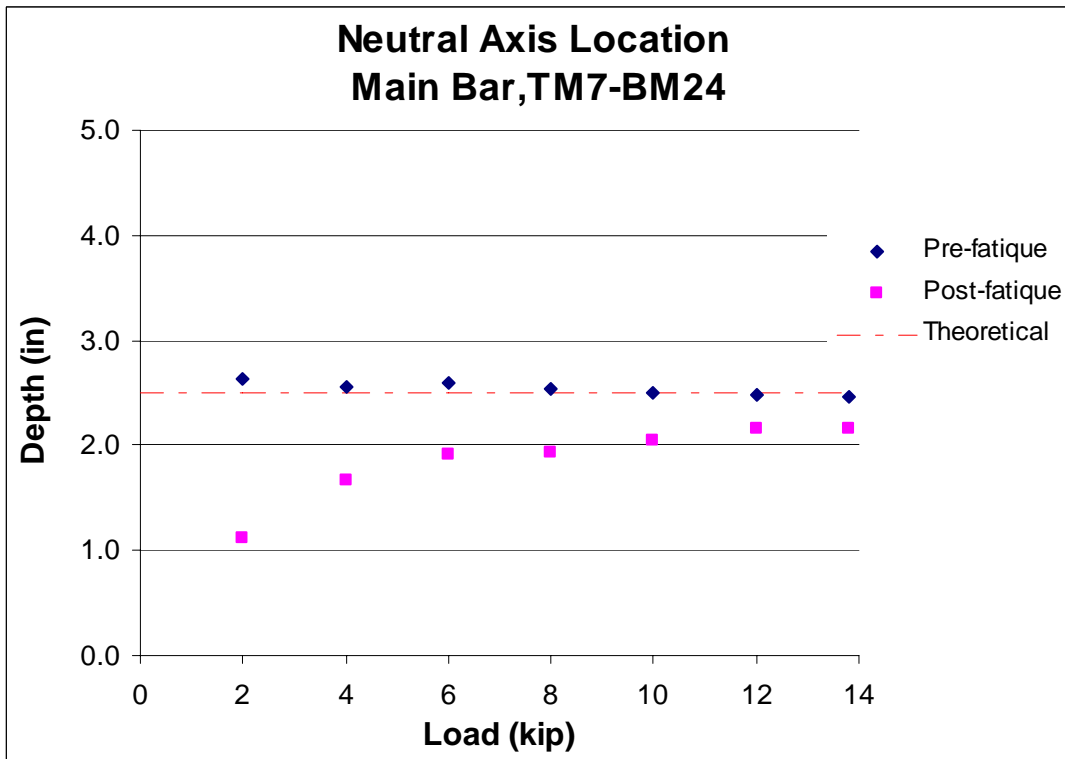


Figure C11 – Main Bar Neutral Axis Location: TM7-BM24

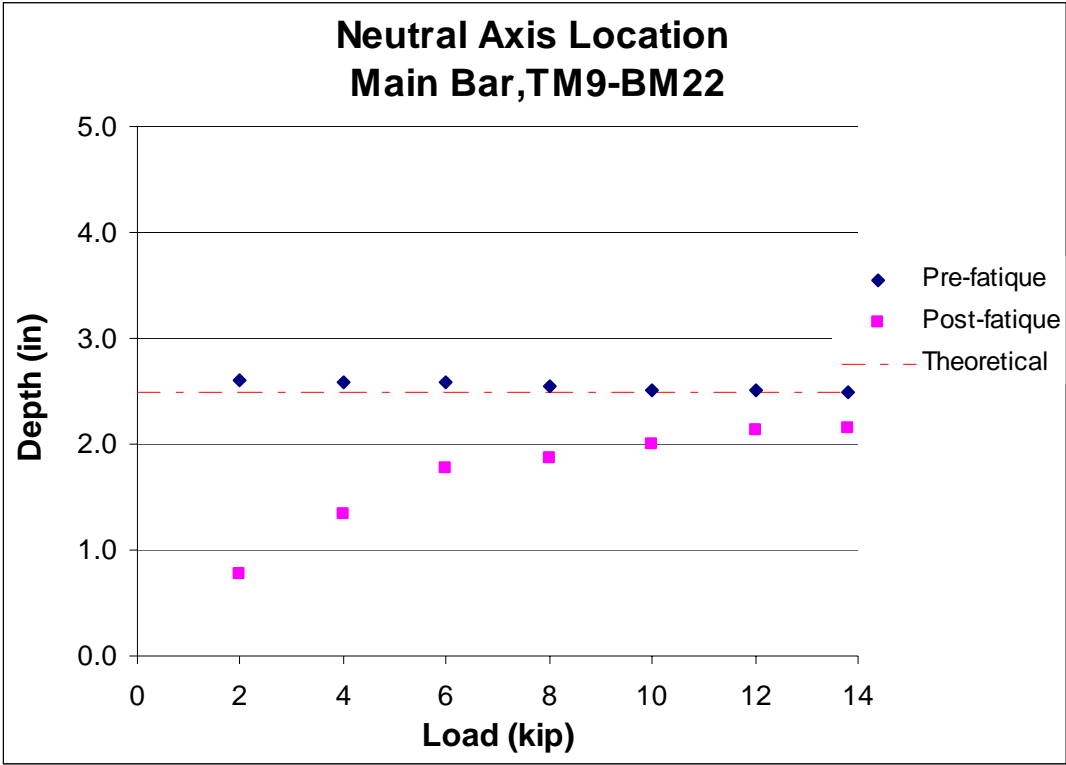


Figure C12 – Main Bar Neutral Axis Location: TM9-BM22

**Table C7 – Main Bar Neutral Axis Data: TM10-BM21**

<u>Gauge</u>	<i>Main Bar</i>		
<u>TM10-BM21</u>	Pre-fatigue	Post-fatigue	Theoretical
	Load	Location	Location
	0		2.5
	2	2.4679	0.8334
	4	2.382	1.2425
	6	2.3671	1.5884
	8	2.2937	1.553
	10	2.2304	1.6928
	12	2.2279	1.8194
	13.8	2.1985	1.8536

**Table C8 – Main Bar Neutral Axis Data: TM13-BM18**

<u>Gauge</u>	<i>Main Bar</i>		
<u>TM13-BM18</u>	Pre-fatigue	Post-fatigue	Theoretical
	Load	Location	Location
	0		2.5
	2	2.5853	0.6433
	4	2.496	1.0304
	6	2.5949	1.3655
	8	2.5066	1.3868
	10	2.3881	1.4819
	12	2.4071	1.791
	13.8	2.3962	1.8285

**Table C9 – Main Bar Neutral Axis Data: TM15-BM16**

<u>Gauge</u>	<i>Main Bar</i>		
<u>TM15-BM16</u>	Pre-fatigue	Post-fatigue	Theoretical
	Load	Location	Location
	0		2.5
	2	2.6934	0.7038
	4	2.5253	1.0096
	6	2.6719	1.3701
	8	2.5699	1.3344
	10	2.4547	1.4528
	12	2.4302	1.7861
	13.8	2.4267	1.7973

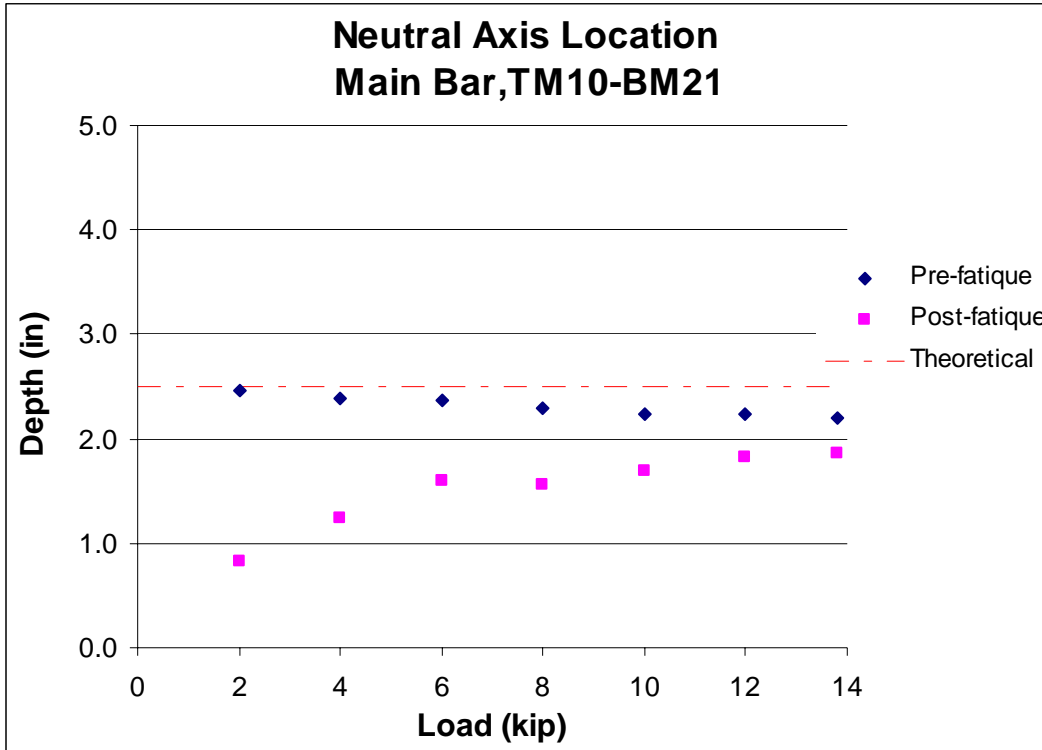


Figure C13 – Main Bar Neutral Axis Location: TM10-BM21

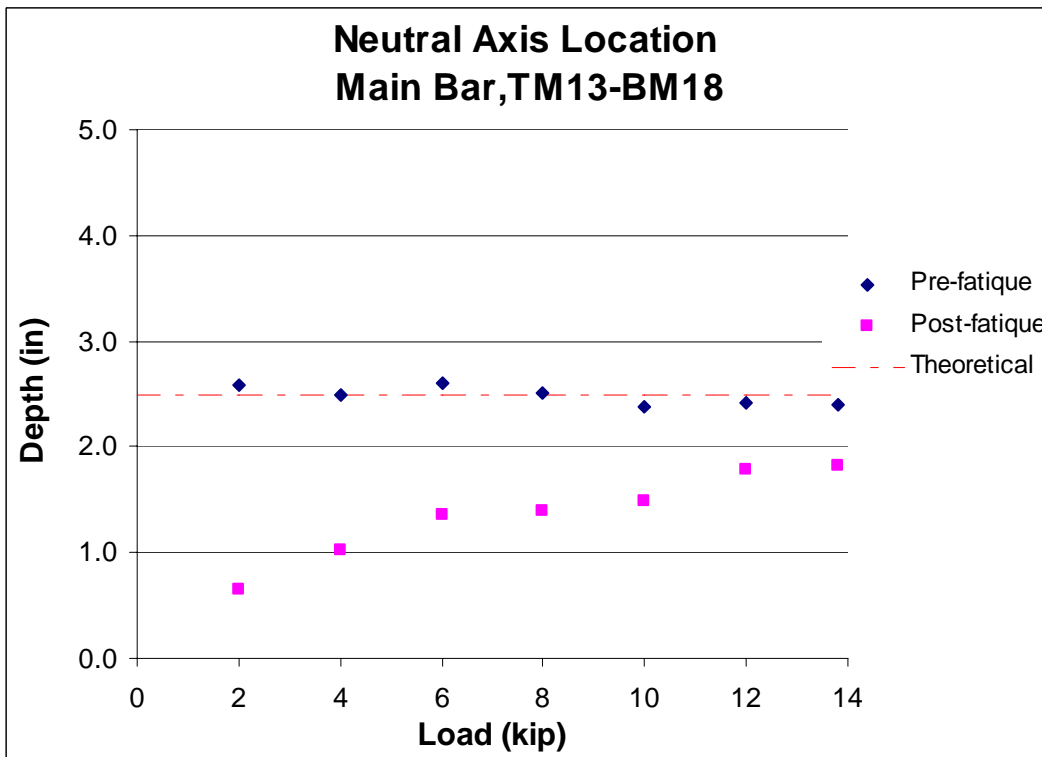


Figure C14 – Main Bar Neutral Axis Location: TM13-BM18

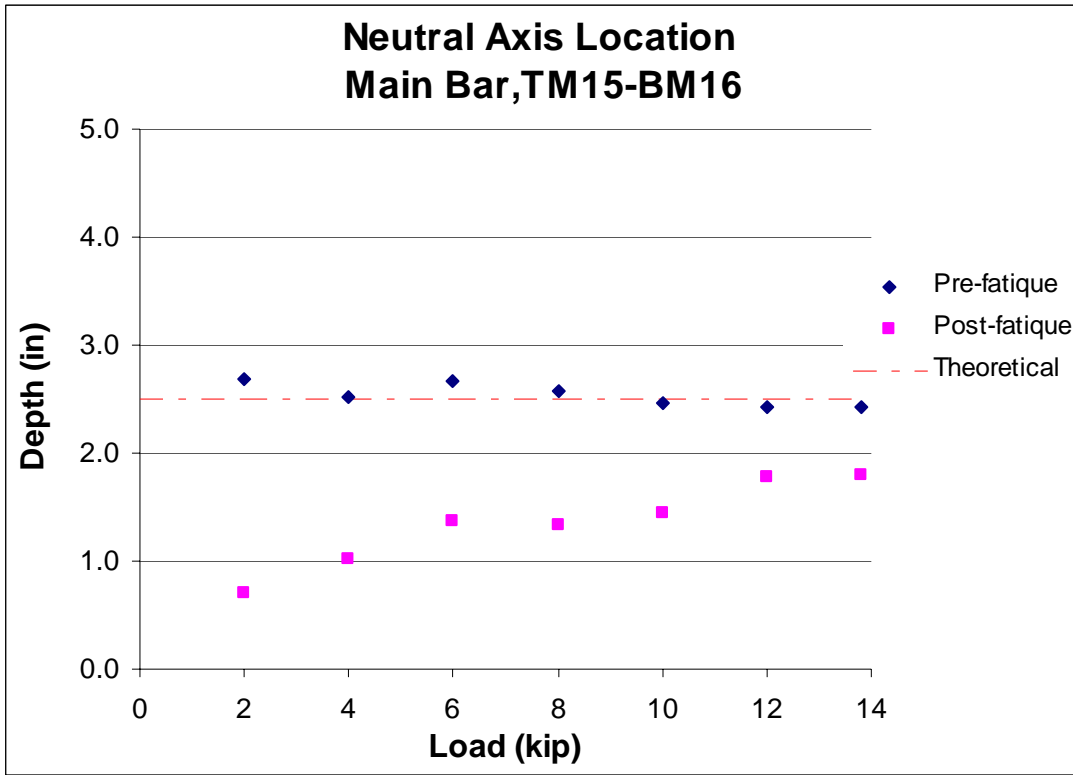


Figure C15 – Main Bar Neutral Axis Location: TM15-BM16

## CROSS BAR STRAIN GAUGE AND N.A. LOCATION DATA

**Table C10 – Pre- and Post-Fatigue Cross Bar Strains  
(Gauges not shown indicate their data was unusable for the applicable analysis)**

Pre-Fatigue			Cross Bar Strains (micro-strain)							
Cross Bar Locations	Depth	Load (kips)								
		0	2	4	6	8	10	12	13.8	
TC 2	2.5	0.00E+00	-1.42E+00	-2.36E+00	-4.73E+00	-7.56E+00	-9.45E+00	-1.09E+01	-1.28E+01	
BC 29	0	0.00E+00	7.59E+00	1.19E+01	1.42E+01	1.71E+01	1.76E+01	1.95E+01	1.99E+01	
TC 5	2.5	0.00E+00	-6.18E+00	-1.19E+01	-1.90E+01	-2.57E+01	-3.23E+01	-3.90E+01	-4.28E+01	
BC 26	0	0.00E+00	1.19E+01	2.38E+01	3.37E+01	4.32E+01	5.04E+01	5.75E+01	6.37E+01	
TC 8	2.25	0.00E+00	-1.37E+01	-2.88E+01	-4.30E+01	-5.91E+01	-7.71E+01	-9.31E+01	-1.10E+02	
TC 8	2.5	0.00E+00	-1.88E+01	-3.93E+01	-5.87E+01	-8.01E+01	-1.03E+02	-1.25E+02	-1.46E+02	
BC 23	0	0.00E+00	3.18E+01	6.55E+01	9.77E+01	1.29E+02	1.59E+02	1.91E+02	2.19E+02	
TC 11	2.5	0.00E+00	0.00E+00	0.00E+00	0.00E+00	0.00E+00	0.00E+00	0.00E+00	0.00E+00	
BC 20	0	0.00E+00	0.00E+00	0.00E+00	0.00E+00	0.00E+00	0.00E+00	0.00E+00	0.00E+00	
TC 14	2.5	0.00E+00	-4.73E-01	4.73E-01	2.37E+00	1.42E+00	-9.46E-01	-9.46E-01	-1.42E+00	
BC 17	0	0.00E+00	2.84E+00	6.15E+00	1.23E+01	1.47E+01	1.51E+01	1.80E+01	2.13E+01	
Post-Fatigue			Cross Bar Strains (micro-strain)							
Cross Bar Locations	Depth	Load (kips)								
		0	2	4	6	8	10	12	13.8	
TC 2	2.5	0.00E+00	-9.45E+00	-1.47E+01	-1.80E+01	-2.50E+01	-2.74E+01	-2.55E+01	-3.02E+01	
BC 29	0	0.00E+00	-5.22E+00	-6.17E+00	-1.42E+00	-3.32E+00	-1.90E+00	2.37E+00	2.85E+00	
TC 5	2.5	0.00E+00	-1.57E+01	-2.71E+01	-3.28E+01	-4.66E+01	-5.37E+01	-5.56E+01	-6.56E+01	
BC 26	0	0.00E+00	2.85E+00	8.55E+00	2.00E+01	2.57E+01	3.23E+01	4.37E+01	4.80E+01	
TC 8	2.25	0.00E+00	-2.32E+01	-4.21E+01	-5.67E+01	-7.80E+01	-9.27E+01	-1.06E+02	-1.21E+02	
TC 8	2.5	0.00E+00	-2.76E+01	-5.13E+01	-7.08E+01	-9.74E+01	-1.17E+02	-1.35E+02	-1.55E+02	
BC 23	0	0.00E+00	1.66E+01	4.08E+01	6.97E+01	9.67E+01	1.25E+02	1.57E+02	1.82E+02	
TC 11	2.5	0.00E+00	0.00E+00	0.00E+00	0.00E+00	0.00E+00	0.00E+00	0.00E+00	0.00E+00	
BC 20	0	0.00E+00	1.62E+02	1.66E+02	-2.90E+02	1.92E+02	-4.69E+01	-2.28E+02	1.07E+02	
TC 14	2.5	0.00E+00	-1.18E+01	-1.61E+01	-1.70E+01	-2.41E+01	-2.60E+01	-2.13E+01	-2.32E+01	
BC 17	0	0.00E+00	-6.15E+00	-7.57E+00	-5.68E+00	-8.05E+00	-8.99E+00	4.73E-01	1.89E+00	

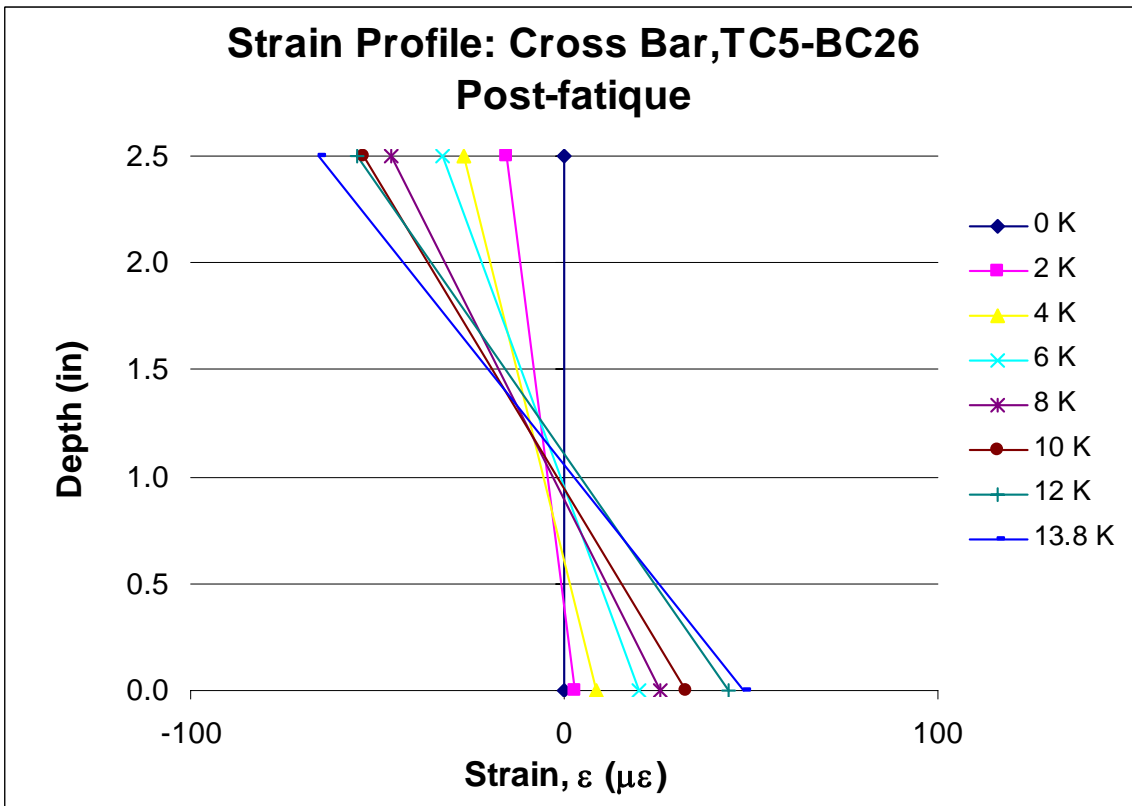
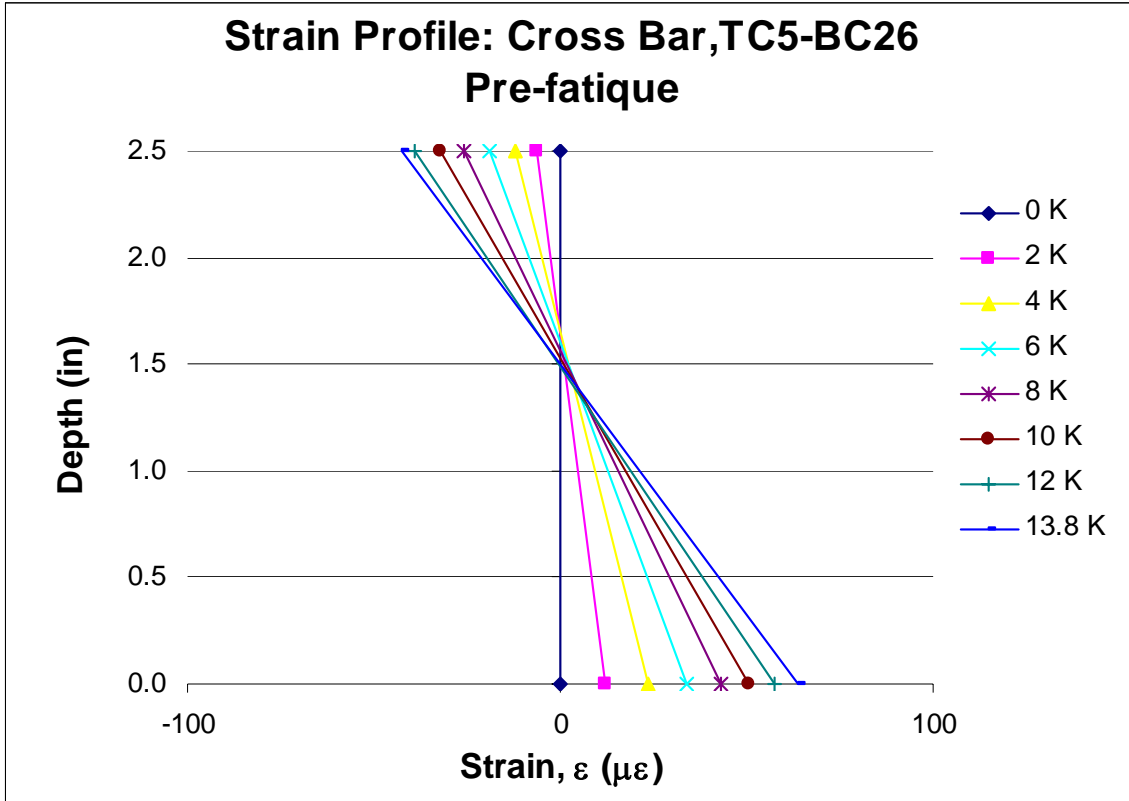


Figure C16 – Strain Profiles: Cross Bar, TC5-BC26

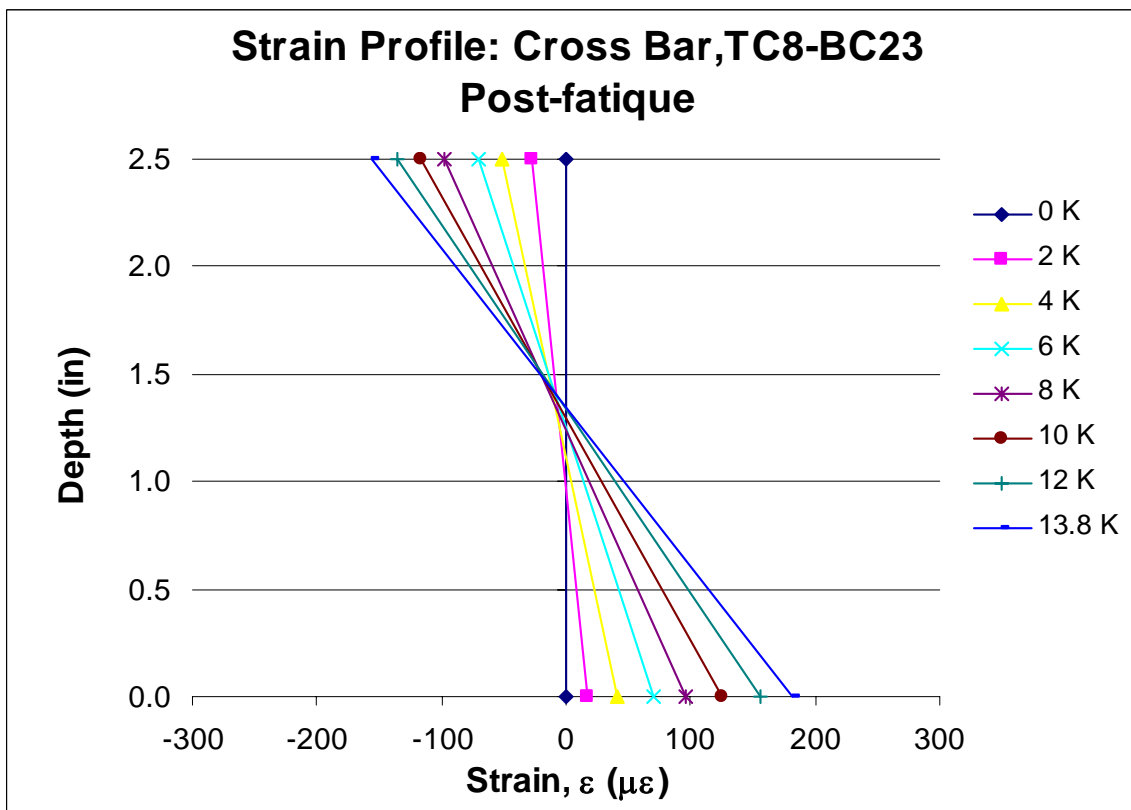
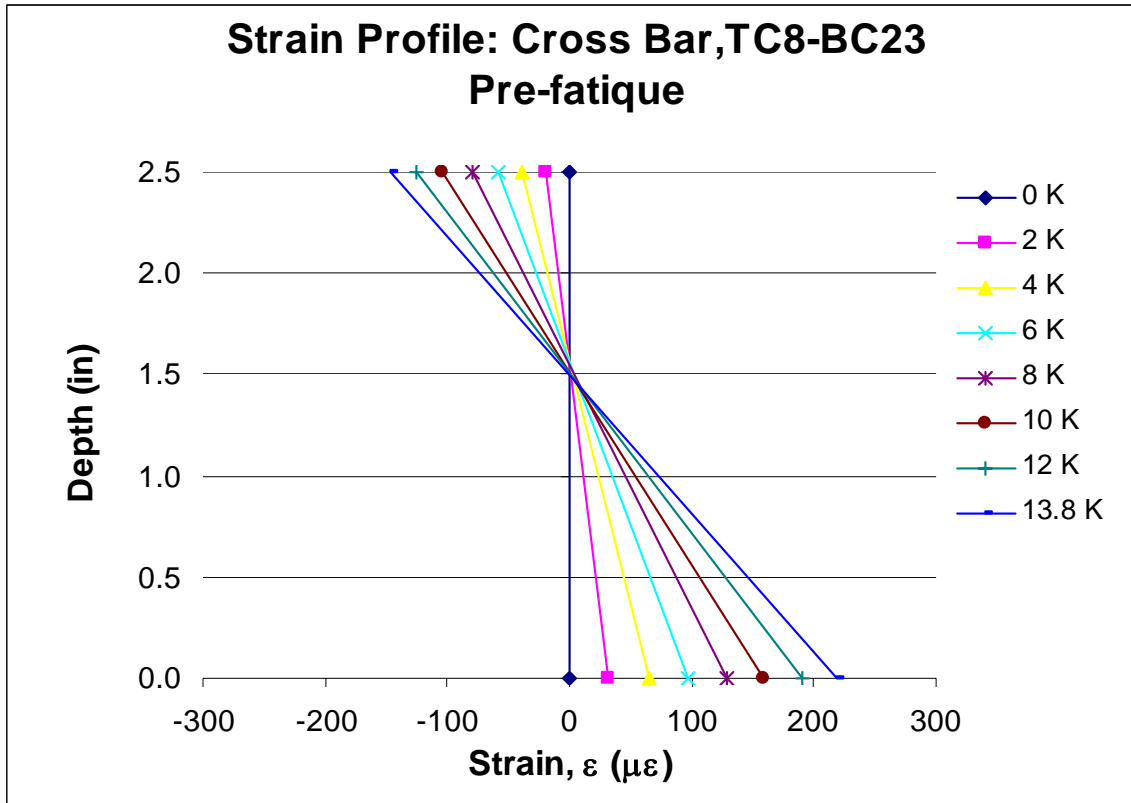


Figure C17 – Strain Profiles: Cross Bar, TC8-BC23

**Table C11 – Cross Bar Neutral Axis Data: TC5-BC26**

<u>Gauge</u> <u>TC5-BC26</u>	<b><i>Cross Bar</i></b>		
	Pre-fatigue	Post-fatigue	Theoretical
Load	Location	Location	Location
0			1.25
2	1.6448	0.3848	1.25
4	1.6668	0.6002	1.25
6	1.5992	0.9462	1.25
8	1.5691	0.8884	1.25
10	1.5231	0.9395	1.25
12	1.4903	1.1008	1.25
13.8	1.4957	1.0568	1.25

**Table C12 – Cross Bar Neutral Axis Data: TC8-BC23**

<u>Gauge</u> <u>TC8-BC23</u>	<b><i>Cross Bar</i></b>		
	Pre-fatigue	Post-fatigue	Theoretical
Load	Location	Location	Location
0			1.25
2	1.5718	0.9392	1.25
4	1.5618	1.1075	1.25
6	1.5621	1.2405	1.25
8	1.5449	1.2457	1.25
10	1.5166	1.293	1.25
12	1.5129	1.342	1.25
13.8	1.4995	1.3497	1.25

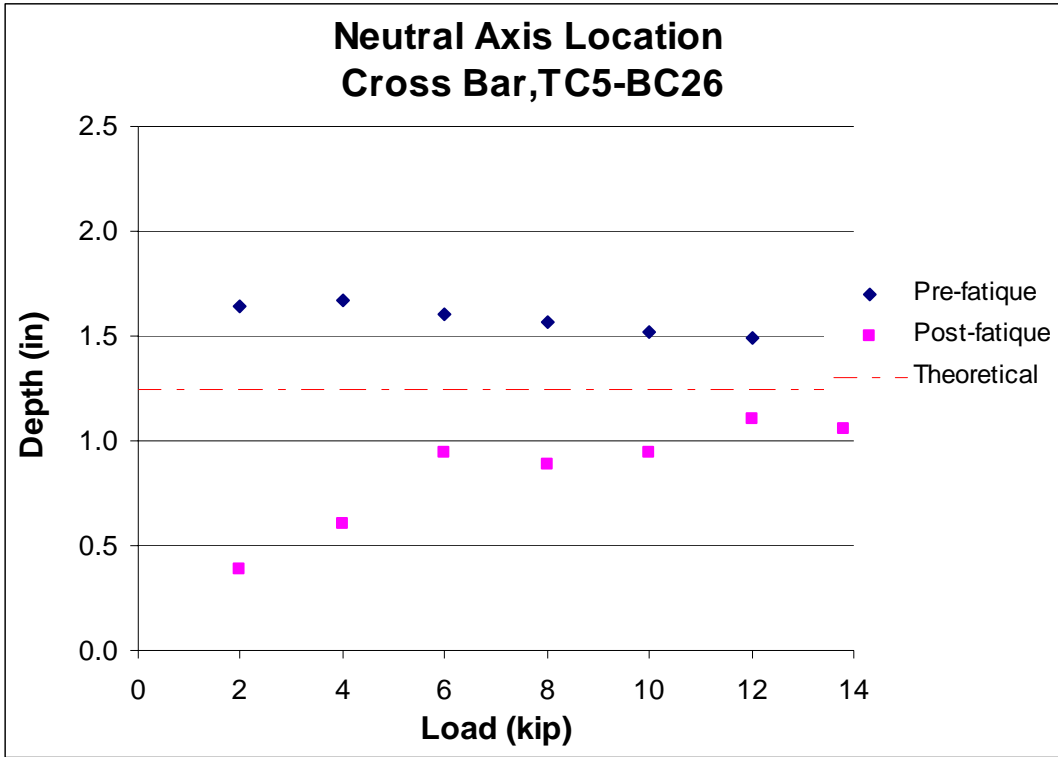


Figure C18 – Cross Bar Neutral Axis Location: TC5-BC26

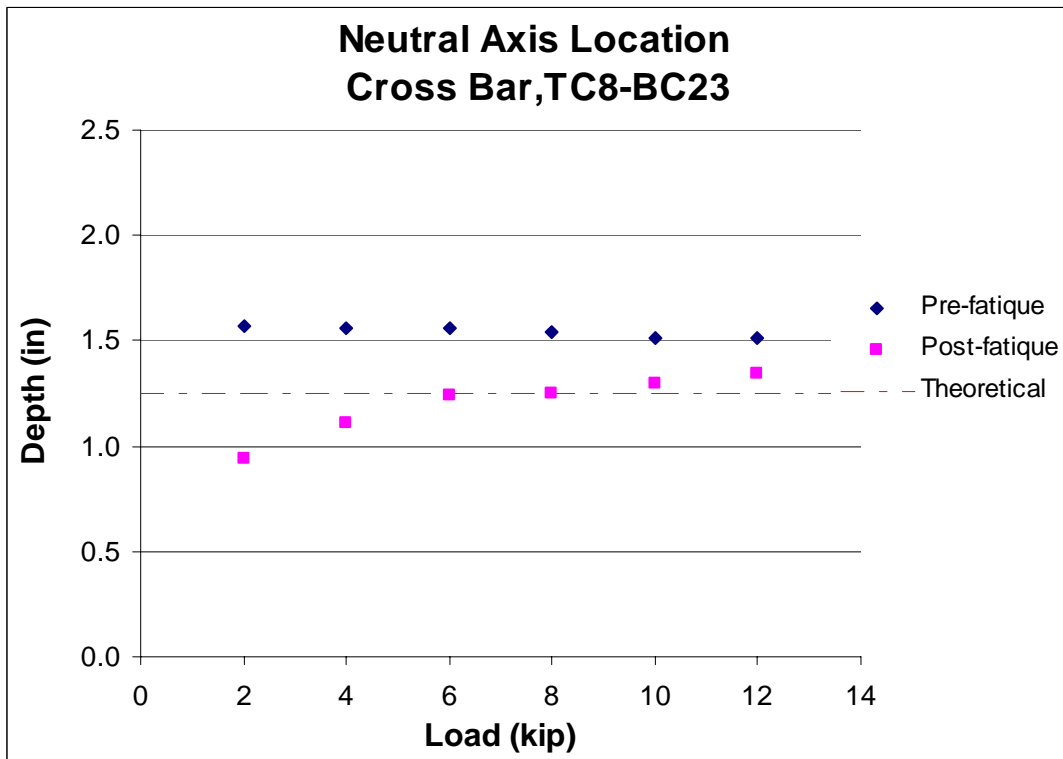


Figure C19 – Cross Bar Neutral Axis Location: TC8-BC23

## BIBLIOGRAPHY

- Pierce, Matthew J., et al. "Evaluative Testing of a Novel Weld-less Open Steel Grid Deck System." University of Pittsburgh, International Bridge Conference – Proceedings, 2001 (IBC-01-10).
- Gilmore, Gene R. "Steel-grid Bridge Flooring: New Innovations to Prove Modular Decking System." National Engineering Conference & Conference of Operating Personnel – Proceedings, 1987.
- Klippstein, Karl H. "Static and Fatigue Strength Determination of Design Properties for Grid Bridge Decks, Volume III – Fatigue Tests and Strain Measurements on Grid Decks." Research Report ST-14, Department of Civil Engineering, University of Pittsburgh, February 1993.
- Mangelsdorf, C.P. "Static and Fatigue Strength Determination of Design Properties for Grid Bridge Decks, Volume II – Plate Stiffness Summary and Strain Measurements on Grid Decks." Research Report ST-10, Department of Civil Engineering, University of Pittsburgh, December 1991.
- Huang, Haoxiong. "Behavior of Steel Grid Decks for Bridges." Doctor of Philosophy Dissertation, University of Delaware, 2001.
- Skroback, K. "An Experimental Study of the Structural Behavior of Open Steel Grid Decks for Bridges." Master Thesis, University of Delaware, 1999.
- Mangelsdorf, C.P. "Static and Fatigue Strength Determination of Design Properties for Grid Bridge Decks, Volume IV – Summary and Final Report." Department of Civil Engineering, University of Pittsburgh, January 1996.